IEEE Open Journal of
Industry Applications

Received 23 August 2021; revised 6 December 2021; accepted 14 December 2021. Date of publication 23 December 2021; date of current version 13 January 2022. The review of this article was arranged by Associate Editor Shafiq Odhano.

Digital Object Identifier 10.1109/OJIA.2021.3137589

State of the Art of Repetitive Control in Power Electronics and Drive Applications

MI TANG [1] (Member, IEEE), MARCO DI BENEDETTO [2] (Member, IEEE), STEFANO BIFARETTI [3] (Member, IEEE), ALESSANDRO LIDOZZI [2] (Member, IEEE), AND PERICLE ZANCHETTA [4,5] (Fellow, IEEE)

[1]Power Electronics, Machine and Control Group, University of Nottingham, NG7 2GT Nottingham, UK
[2]Roma Tre University C-PED, Center for Power Electronics and Drives, 00154 Rome, Italy
[3]Department of Industrial Engineering, University of Rome "Tor Vergata", 00133 Rome, Italy
[4]Department of Electrical and Electronic Engineering, University of Nottingham, NG7 2RD Nottingham, UK
[5]Department of Electrical, Computer and Biomedical Engineering, University of Pavia, 27100 Pavia, Italy

CORRESPONDING AUTHOR: Mi Tang (e-mail: mi.tang2@nottingham.ac.uk)

ABSTRACT Power electronic systems present a non-linear behavior mainly due to their switching nature. This is often combined with their interaction with non-linear systems, such as other switching converters, diode rectifiers, motor drives, etc. and with possible non linearities of the power grid in the case of grid connected systems. The major effect of these non-linear interactions is the generation of harmonic distortion on voltages and currents (both in DC and AC), which needs to be compensated to achieve high power quality systems. The use of passive filters is often the simplest and most immediate solution; however, this decreases converter efficiency and increases its weight and volume. Thus, the use of a control strategy capable of tracking periodic signals, rejecting periodic disturbance and largely improving steady state behavior and harmonic distortion with a limited bandwidth is a very desirable feature. Repetitive Control (RC) represents an extremely practical and efficient solution for the aforementioned issues, and it is widely employed in many different applications. This paper focuses on state of the art of RC used in power electronics and drives. RC basic concepts, different control structures, design methods, fixed and variable frequency operating conditions, etc. are investigated. Furthermore, many example applications and existing control approaches developed in recent years for power electronics and drive systems based on RC, have also been discussed in detail.

INDEX TERMS Repetitive control, control design, reviews, power electronic converters, electric drives, grid-tied, off grid.

I. INTRODUCTION

The tracking of periodic signals and rejection of periodic disturbances in a control system is a wide field of research both in control theory and many application areas. Over the years, RC has proven to be an excellent technique to address this issue [1]. In fact nowadays, RC is successfully used in many real-world control applications, such as robotics [3], [4], electro-hydraulics [5], tubular heat exchangers [6], PWM converter [1], [7]–[50], etc. RC was introduced for the first time by Hara, Yamamoto, Omata and Nakano and it is based on the Internal Model Principle (IMP) [2]. The implementation of RC requires the controller to incorporate a model of the dynamics that generate the signals which the control system is intended to track/reject. If the periodic reference signal is composed by a certain number of frequencies, the RC will contain all periodic modes, whose number is proportional to the period T_p and inversely proportional of the sampling interval T_s (Hara *et al.*, 1988). This results in a very high order control system, particularly when the sampling frequency ($f_s = 1/T_s$) is high. The RC is practically designed considering a constant sampling period T_s and assuming a constant period T_p for the signals to be tracked/rejected, such that the ratio $N = T_p/T_s$ is embedded in the control algorithm. However, the frequency of the tracked signals ($f_p = 1/T_p$) is not perfectly constant in many practical applications, as well as the disturbance period can change according to the

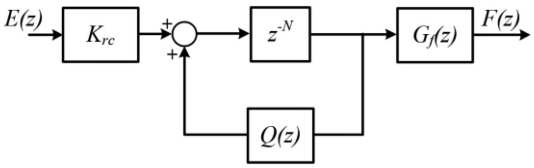

FIGURE 1. Block diagram of a standard RC.

speed variations in rotational mechanical systems (peristaltic pumps, machining tools, etc.), and frequency variations of the power devices (inverters, rectifiers, etc.) connected to the electric distribution network [10], [11]. This problem leads to a dramatic decay of the controller performance [12]. To overcome this problem several papers have appeared in literature [4], [13]–[19], which propose two different kind of approaches : 1) variable value of N and 2) fixed value of N.

The first consists in keeping the sampling period T_s constant and change the value of N according to the time variation of T_p [4], [13]. Another solution within approach 1 is to adapt the controller sampling rate according to the reference/disturbance period [14]. This enables to obtain good performance in the steady state while maintaining low computational burden. Approach 2 works with a fixed value of N and the frequency variations are compensated by means of large memory elements [12]. This method works well, as long as the frequency variations is small, with high computational complexity. An alternative simpler method, still falling within approach 2, is to use a fictitious sampler operating at a variable sampling rate [6], [15], [16]. Compared to the previous method, in this case the performance is slightly degraded, but the computational burden is lower.

This paper aims to provide a thorough and comprehensive review of RC, its design methodology and its more recent applications in power electronics and drives. The outline is as follows: Section II provides the operating principles of RC, while Section III illustrates the design methodology. Section IV investigates solutions for variable frequency implementation; Section V analyses the concept of assisted repetitive control, while Section VI introduces a high number of practical examples both in power electronics and drives, some including experimental results. Open issues and further work are discussed in Section VII and conclusions are drawn in Section VIII.

II. BASIC PRINCIPLE OF REPETITIVE CONTROL

A. BASICS OF A REPETITIVE CONTROLLER

The block diagram of a standard RC can be seen in Fig. 1, where the input signal E is assumed to be a periodic signal with period equal to T_d. F is a compensation action; K_{rc} is the gain of RC; the long delay chain z^{-N} ideally should provide a delay of T_d, so N is calculated by rounding the ratio between T_d and the sampling period T_s to the closest integer. NT_s is the learning period of RC. $Q(z)$ is the robustness filter used (usually a low pass filter) to attenuate the effect of any high frequency noise presents in E. $G_f(z)$ is namely the stability filter, which is often used to compensate any delay in the acquisition of E [7], [13], [15].

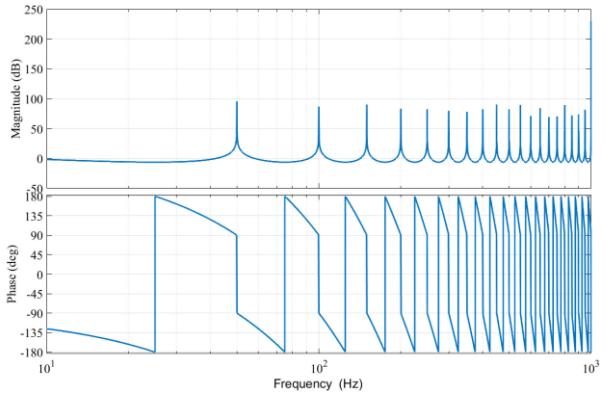

FIGURE 2. Bode plot of the RC with $K_{rc} = 1$, $G_f(z) = 1$, $Q(z) = 1$ and $N = T_d/T_s = 400$.

The transfer function of RC can be represented in (1).

$$G_{RC}(z) = \frac{F(z)}{E(z)} = \frac{K_{rc} G_f(z) z^{-N}}{1 - Q(z) z^{-N}}. \tag{1}$$

Popular choices of $Q(z)$ include the forgetting factor (i.e., a constant between zero and one) and a moving average filter which passes medium and low frequencies, but attenuates high frequencies [17]. $G_f(z)$ can be chosen as a zero-phase error tracking compensator, originally proposed by Tomizuka in 1985 for servo drive [20], which is essentially the reverse of the plant seen by the RC. Alternatively, when the plant seen by RC is a fixed delay, $G_f(z)$ can be a simple a phase lead compensator as in [21], z^M, where MT_s equals the fixed delay time. Fig. 2 shows the Bode plot of the RC transfer function given in (1), when $K_{rc} = 1$, $G_f(z) = 1$, $Q(z) = 1$ and $N = T_d/T_s = 400$. In this case, the delay time T_d is equal to 20ms and the sampling period T_s is equal to 50μs. It can be noticed that the response presents high gain at fundamental and desired periodic frequencies, while the phase is equal to 0° to the fundamental frequency and its multiples.

B. PLANT SEEN BY A REPETITIVE CONTROLLER

As mentioned above, the choice of $G_f(z)$ depends on namely the "plant seen by the RC". Depending on how the RC is connected in the feedback loop, it sees the plant differently. As shown in Fig. 3, three are the most common structures used for connecting the RC into a control system: direct, parallel, and plug-in [22]–[24]. In Fig. 3, $R(z)$ is the reference, $E(z)$ is the error between reference $R(z)$ and feedback $Y(z)$, $F(z)$ is the compensation action generated by the RC. $U(z)$ is the input to the plant G_P, $D(z)$ is the disturbance and G_C is the feedback controller. No matter which structure is used, the closed loop system can be re-drawn into an equivalent diagram as in Fig. 4, where G_{PRC} is defined as the plant seen by RC. It can then be derived that the "plant seen by RC", G_{PRC}, is given in

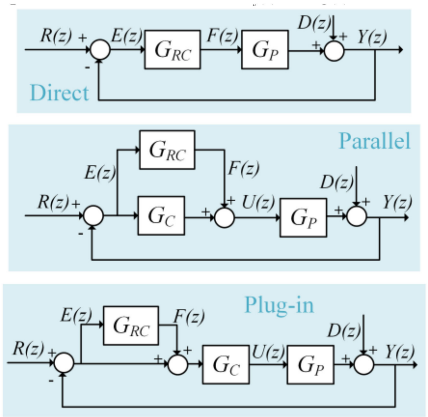

FIGURE 3. Three typical structures for RC.

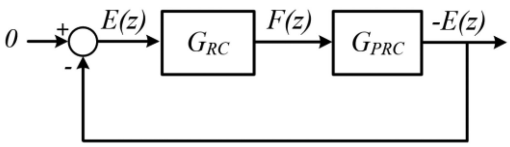

FIGURE 4. Equivalent diagram for the plant seen by RC.

(2) according to the three structures of Fig. 3.

$$G_{PRC} = \frac{-E(z)}{F(z)} = \begin{cases} G_P, & \text{direct} \\ \frac{G_P}{1+G_C G_P}, & \text{parallel} \\ \frac{G_C G_P}{1+G_C G_P}, & \text{plug}-\text{in}. \end{cases} \tag{2}$$

C. THE RC WORKING PRINCIPLE

The fact that RC can ideally cancel periodic errors can be proven by finding the zero error tracking conditions [1]–[3]. Hence, the transfer function of the error $E(z)$ is derived as in (3).

$$E(z) = \begin{cases} \text{direct: } \frac{(1-Q(z)z^{-N})(R(z)-D(z))}{1-z^{-N}(Q(z)-K_{rc}G_f(z)G_P(z))} \\ \text{parallel:} \\ \frac{(1-Q(z)z^{-N})(R(z)-D(z))}{(1+G_C(z)G_P(z))\left[1-z^{-N}\left(Q(z)-\frac{K_{rc}G_f(z)G_P(z)}{1+G_C(z)G_P(z)}\right)\right]} \\ \text{plug-in:} \\ \frac{(1-Q(z)z^{-N})(R(z)-D(z))}{(1+G_C(z)G_P(z))\left[1-z^{-N}\left(Q(z)-\frac{K_{rc}G_f(z)G_C(z)G_P(z)}{1+G_C(z)G_P(z)}\right)\right]} \end{cases} \tag{3}$$

Substituting z with $e^{j\omega T_s}$, the numerator of (3) becomes $(1 - Q(e^{j\omega T_s}))e^{-j\omega N T_s}[R(e^{j\omega T_s}) - D(e^{j\omega T_s})]$, where, $NT_s = T_d$, as defined in Section II-A. Assuming the robustness filter $Q(e^{j\omega T_s}) = 1$, the error signal E equals zero when the angular frequency ω satisfies the condition in (4).

$$\omega = \omega_d = \frac{2k\pi}{T_d} < \omega_{nyq} \forall k = 0, 1, 2 \ldots k_{\max}$$

TABLE I Definition of $G_{S1}(z)$, $G_{S2}(z)$, $G_{S3}(z)$

Type	$G_{S1}(z)$	$G_{S2}(z)$	$G_{S3}(z)$
Direct	$1-Q(z)z^{-N}$	Not Available	$Q(z)-K_{rc}G_f(z)G_P(z)$
Parallel		$\frac{1}{1+G_C(z)G_P(z)}$	$Q(z)-\frac{K_{rc}G_f(z)G_P(z)}{1+G_C(z)G_P(z)}$
Plug-in			$Q(z)-\frac{K_{rc}G_f(z)G_C(z)G_P(z)}{1+G_C(z)G_P(z)}$

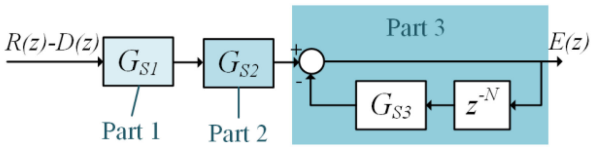

FIGURE 5. Equivalent block diagram of Fig. 4 according to (4).

$$\begin{cases} k_{\max} = \frac{N-1}{2} \text{for odd } N \\ k_{\max} = \frac{N}{2} \text{for even } N \end{cases} \tag{4}$$

where, ω_N is the Nyquist frequency in rad/s $2\pi f_s/2$. This means that, with RC, all signals of frequency $1/T_d$ and its integer multiples will either be tracked if contained in R or suppressed if received from D up to the Nyquist frequency.

D. STABILITY CONDITIONS

Before RC can be applied, the stability of the overall system with RC needs to be analysed. Although the stability conditions for an RC system can be derived based on Routh-Hurwitz criterion [23], Lyapunov stability [26]–[28], H-infinity control [29]–[30], Nyquist stability criterion [31], pole placement [32] and other optimization methods in robust control [33]–[34], one of the simplest methods is based on the small gain theorem [35]–[37]. An equivalent block diagram and Table I can be derived according to (4).

As drawn in Fig. 5, the whole RC system can be divided into three parts. Hence, the stability of the RC system can be ensured if each part is stable. According to the small gain theorem, the stability of each part can be guaranteed if its input is bounded and the loop gain is smaller than unity, i.e., $|G_{S1}(z)| < 1, |G_{S2}(z)| < 1, |G_{S3}(z)| < 1$.

The first part is always stable since the robustness filter $Q(z)$ as introduced in Section II-A has its gain lower than one. The second part, only available for the parallel and plug-in types of RC, will be stable once the closed loop without RC has been designed stable. The third part will be stable if the condition

in (5) is satisfied.

$$\left.\begin{array}{l}\text{direct}: \\ \left|Q(e^{j\omega T_s}) - K_{rc}G_f(e^{j\omega T_s})G_P(e^{j\omega T_s})\right| < 1 \\ \text{parallel}: \\ \left|Q(e^{j\omega T_s}) - \frac{K_{rc}G_f(e^{j\omega T_s})G_P(e^{j\omega T_s})}{1+G_C(e^{j\omega T_s})G_P(e^{j\omega T_s})}\right| < 1 \\ \text{plug-in}: \\ \left|Q(e^{j\omega T_s}) - \frac{K_{rc}G_f(e^{j\omega T_s})G_C(e^{j\omega T_s})G_P(e^{j\omega T_s})}{1+G_C(e^{j\omega T_s})G_P(e^{j\omega T_s})}\right| < 1.\end{array}\right\} \forall\omega \in [0, \omega_{nyq}] \tag{5}$$

III. DESIGN AND IMPLEMENTATION

A. SELECTION OF ROBUSTNESS FILTER

An ideal RC has high gains in the high frequency region as in Fig. 2. In reality, such high gains at high frequency leads to high sensitivity against high frequency uncertainties such as noise. Hence, the high frequency gains need to be attenuated by selecting the robustness filter as a close-to-unity constant or a moving average filter. The differences are described as below:

1) CLOSE-TO-UNITY CONSTANT

Selecting the Q(z) as a close-to-unity gain effectively attenuates equally all gains for all frequencies. It is a simple solution, but it will introduce a higher error E defined in (3).

2) MOVING AVERAGE FILTER

Selecting the Q(z) as a moving average filter will attenuates only the high frequency gains while keeping unaltered the low frequency gains. The selection of moving average filer is based on the system model accuracy [38]. A poor modeling at high frequency requires a strict filter design with low cut-off frequency.

B. PHASE COMPENSATION

The stability filter $G_f(z)$ can be selected to achieve the zero-phase error-tracking compensator if an accurate plant model is obtained [39], such that the stability filter can be chosen according to the reverse of the plant seen by RC as derived in Section II-B. However, due to various uncertainties and load disturbance in the feedback system, the phase-lead compensation is designed as in (6), where M is the prediction index.

$$G_f(z) = z^M. \tag{6}$$

The phase-lead term z^M can reach Nyquist frequency ω_N at $M{\cdot}180°$, and it provides a phase lead $\theta = M{\cdot}180°{\cdot}(\omega/\omega_N)$ to compensate the system phase lag. Consequently, using an appropriate prediction index M, the delays of the feedback control system can be compensated. This enables using the RC to eliminate the effects of control delays. If the RC and the rest of the control system are running at different sampling rate, the phase compensation can be designed as in [40].

C. FRACTIONAL DELAY ISSUE

The fractional delay issue is known as a performance degradation of RC due to the mismatch between the real period T_d of the periodic signal and the learning period NT_s of RC. Since N can only be an integer, if T_d/T_s is a fractional number, RC may not "learn" the periodic signal accurately. To improve the resolution of the RC, a Lagrange interpolation based RC is presented for active filters [16], inverters [8], [14], [39] and phase locked loops [41].

$$x(k-N) = \sum_{j=0}^{n} P_j x(k - N_i - j)$$
$$\text{for } P_j = \prod_{\substack{h=0 \\ h\neq j}}^{n} \frac{N_f - h}{j - h} \forall j = 0, 1, \ldots, n. \tag{7}$$

For example, N can be expressed by $(N_i + N_f)$, where N_i is the integer portion of N and $0 < N_f < 1$ is the fractional portion. If the order of the Lagrange fractional delay filter is n, in the k^{th} sampling interval, the value of x at $t_{k\text{-}N}$ can be expressed as in (7). More examples of using this filter can be found in the Phase-locked loop application in Section VI-A.

D. IMPLEMENTATION WITH REDUCED MEMORY LENGTH

The length N of the delay chain can be considerably long when R and D are low frequency signals, and the sampling frequency is high. To reduce the memory size and computational resources required for implementation, a Pade-approximation-based RC is proposed in [42] for voltage source inverter, where the long delay chain z^{-N} is estimated by a ninth order Pade approximation. Alternatively, at the cost of losing even-harmonics compensation, memory length of the RC can be reduced to half of the original [43] Running the RC at a down-sampled rate can also reduce the memory length, however it can cause fractional delay issue. The cyclic RC is proposed in [44] to achieve a RC with low-rate output without causing the fractional delay issue by shifting the sampling points within a sampling period.

E. IMPLEMENTATION ON DSP AND LABVIEW FPGA

Industrial grade DSPs are usually the preferred way for control algorithm implementation due to their convenient performance vs. cost ratio. Due to the recent introduction of floating-point units, increased calculation speeds and large memory availability, the RC implementation on a DSP has become really straightforward compared to initial realizations [46]. On the other hand, FPGAs are gaining researchers and industry attention as, due to their capabilities of true parallel operations, are able to obtain significantly reduced execution time, compared to DSPs. In addition, FPGA can enable hardware redundancy required in safety critical and space applications. Two of the most significant FPGA drawbacks, i.e., fixed-point operations and time-consuming implementations,

have been recently overcame by graphical-based programming tools with inherent floating-point usage, e.g., NI LabVIEW FPGA software. Such an approach has been employed, amongst the others, to easily implement direct RC [22] and combined deadbeat and RC [47].

The plug-in RC basic structure, using a fixed delay $G_f(z) = z^M$, can be implemented by using a circular buffer with one N elements vector or equivalently, a pointer to an assigned memory zone, and two indexes k and s, pointing respectively to the current error in the previous fundamental period and to the current error delayed by the compensator delay M. Denoting with E the actual error, $ep[k]$ the k-th element of the error vector, the following calculations have to be performed every control period:

1. define new value for $ep[k] = K_{rc} * (E + ep[k])$;
2. define delayed index s as $k + M$, accounting the buffer circularity;
3. define current value for RC output $F(k)$ as $K_{rc} * ep[s]$;
4. reset index k when $k > N$;

It is worth noting that the previous procedure can be applied by moving, in the block diagram shown in Fig. 1, the gain K_{rc} to the output $F(z)$.

In case of variable frequency operation, N has to be selected on the basis of the lowest operation frequency. For grid-connected converters, which includes the online estimation of the grid parameters, an adaptive adjustment of N can be easily obtained by synchronizing the reset of index k with the zero-crossing of the estimated grid angle. More discussions on the variable frequency operation will be given in the next section.

IV. VARIABLE FREQUENCY OPERATION

For variable frequency operation, this section discusses three typical approaches.

A. VARIABLE SAMPLING PERIOD APPROACH

To keep N fixed, when T_d varies, the sampling period T_s needs to be varied accordingly [17], [18], [48]. To ensure the stability of RC with time-varying sampling period, [48] proposes a robust stability filter when the sampling period varies. It is possible that for some applications, in order to achieve a constant N, a rather large variability of the sampling period is required, and this may not be practical. Hence, authors in [18], combine the variation of sampling frequency f_s and the delay length N. When the frequency of the signal to be tracked varies, in order to maintain a constant value of N, the sampling frequency f_s is varied within a range. When f_s reaches a limit value (lower or upper), N is changed to another constant value (lower or higher, like a gear changing) so to keep f_s within the fixed range. A look/up table for f_s and N is then proposed.

B. VARIABLE DELAY LENGTH APPROACH

When varying the sampling period is not a practical choice, varying N is an option [18], [45]. Both in [18] and [45], the length of the delay chain is updated in every sampling interval. However, in [18], there is no fractional delay issue since authors combine the variation of f_s and N to ensure N is an integer. Otherwise, the fractional delay issue must be addressed to allow continuous varying of N as in [45].

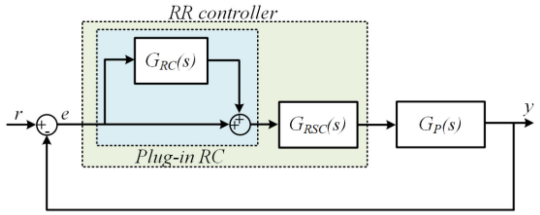

FIGURE 6. Block scheme of RR controller.

C. ANGLE DOMAIN APPROACH

References and Disturbances $(R$ and $D)$ often contain more than one frequency. If the orders of all components in $(R\text{-}D)$ are fixed, the $(R\text{-}D)$ signal will always be periodic with the phase angle of the fundamental component regardless of the variation of its fundamental frequency. Thus, an angle-based RC is proposed in [19]. It is worth noting that the angle-based RC naturally supports fractional delay.

The equations for the angle domain implementation can be found in [19]. An example of its implementation can be seen later in Section VI-B.

V. ASSISTED REPETITIVE CONTROL

A. REPETITIVE CONTROL COMBINED WITH RESONANT CONTROL (RR)

As explained in [49], the RC can be combined with a resonant control structure (RCS) to enhance the tracking performance, the output power quality as well as the system robustness and dynamics. In fact, the RC can compensate a wide range of harmonics up to the Nyquist frequency in a recursive way, but its dynamics is very slow.

Therefore, benefits can be obtained when the RC works in conjunction with RCS that is specifically tuned at the fundamental harmonic. In this case RC and RCS are used in a cascade configuration (indicated in the following as RR), as shown in Fig. 6, where $G_P(s)$ is the plant transfer function, $G_{RSC}(s)$ is the RSC transfer function and G_{RC} is the RC transfer function. The RC TF and RSC TF representations in the s-domain have been obtained in [23]. As it can be seen from Fig. 6, the plug-in RC system is considered [23], [50].

$$G_{RR}(s) = \overbrace{\left(1 + K_{rc}\frac{e^{-T_1 s}}{1 - Qe^{-T_d s}}\right)}^{RCTF} \times \overbrace{\left(2k_{ir}\omega_{cr}\frac{s + \omega_{cr}}{s^2 + 2\omega_{cr}s + \omega_{cr}^2 + \omega_0^2}\right)}^{RSCTF}. \quad (8)$$

The transfer function (TF) of the RR controller can be written as in (8), where T_d is the main delay time (related

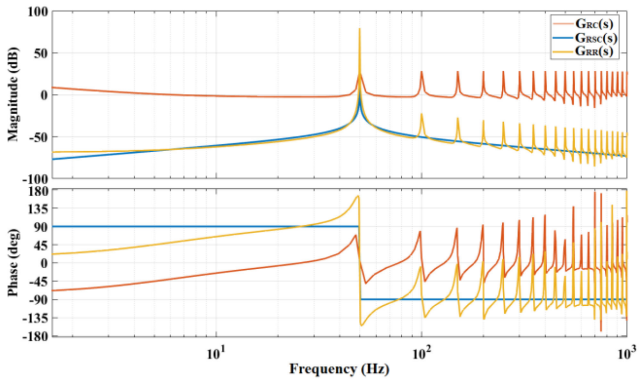

FIGURE 7. Bode plot of the: RC controller (orange line), RSC controller (blue line) and RR controller (gold line).

TABLE II Parameters of the RC and RSC Controllers

RC controller parameters	
K_{RC}	0.5
$Q(z)$	0.98
$G_f(z)$	z^4
f_{sw}	12 kHz
N	240
RSC controller parameters	
k_{ir}	350
ω_{cr}	0.002
ω_0	314

to the fundamental frequency to be tracked), T_1 is the delay time related to the stability filter, K_{rc} is the repetitive learning gain, Q the robustness filter in s-domain, k_{ir} is the controller gain, ω_{cr} is the resonant controller width at -3 dB from the resonance peak and ω_0 is the resonance frequency. Fig. 7 shows the Bode plot of the RC controller (orange line), RSC controller (blue line) and RR controller (gold line) according to the parameters listed in Table II.

As it can be seen from Fig. 7, thanks to the RSC, the RR controller (gold line) has high gain at fundamental frequency compared to the RC regulator and RSC regulator. Consequently, the RR regulator allows to improve the tracking capability regarding to the reference signal variation at low frequency. When the frequency increases, the amplitude of the RR regulator has the same shape as the RC regulator, but with small gains. This means that the high frequency attenuation of the RR regulator provides better stability margins than the single RSC or RC controller without losing the harmonic compensation capability. Equation (8) in the continuous domain cannot be implemented on a digital control system. Thus, the RR regulator can be expressed in the discrete domain as in (9) shown at the bottom of this page, where $G_f(z)$ is the stability filter in z-domain, $Q(z)$ is the robustness filter in z-domain and N is the delay time defined as the ratio between the pulse period T_p and the sampling time T_s. Acting on $G_f(z)$ and $Q(z)$ parameters it is possible to increase the stability margin and stabilize the entire system. The RSC TF in the z-domain can be obtained by Tustin's method with frequency pre-warping,

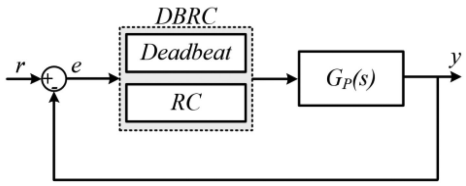

FIGURE 8. Block diagram of DBRC.

which allows to not alter the resonance frequency in z-domain [51].

B. COMBINED DEADBEAT AND REPETITIVE CONTROL (DBRC)

A detailed description of the combined deadbeat (DB) and RC controls [47], [52] is explained in this section. The block diagram of the DBRC is shown in Fig. 8. In this case, the DB control is not used to provide harmonic compensation but, thanks to its high control bandwidth feature, is employed to provide fast dynamic response during the start-up or during transients [47]. The task of the repetitive controller is to provide harmonic compensations and achieve a high performance in the steady state.

C. REPETITIVE CONTROL COMBINED WITH DISTURBANCE OBSERVER

Following the analysis in Section II-D, RC needs to be designed considering the feedback controller G_C. However, as a sibling of RC, the repetitive observer (RO) proposed in [53] merges the traditional RC with a disturbance observer, such that the RO remains functionally the same as RC while it can be designed independently from G_C as a disturbance observer. It has been mathematically proved in [53], [54] that the separation principle of disturbance observer still applies to the RO. As a result, RO offers a wider stability margin than the RC according to [55].

For cases where periodic disturbance needs to be suppressed, RO is an easy-design alternative to RC. The design procedure can be found in [54]. An example of applying RO will be introduced in Section VI-B. In details, a correction term has been added to the RC as in Fig. 9.

VI. APPLICATIONS

RC has been applied in power electronics and drives applications for decades to solve the important issues in the filed such as the distortion of output voltage or current in power supplies (e.g., single-phase flyback inverters [56], [57], single-phase Cuk inverters [58], three-phase inverters [59], [60]), the phase tracking error in grid synchronization and torque, speed or position tracking error in drives. Some examples are introduced in detail as follows.

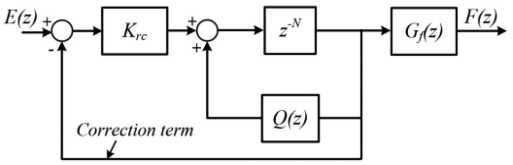

FIGURE 9. Block diagram of a RO.

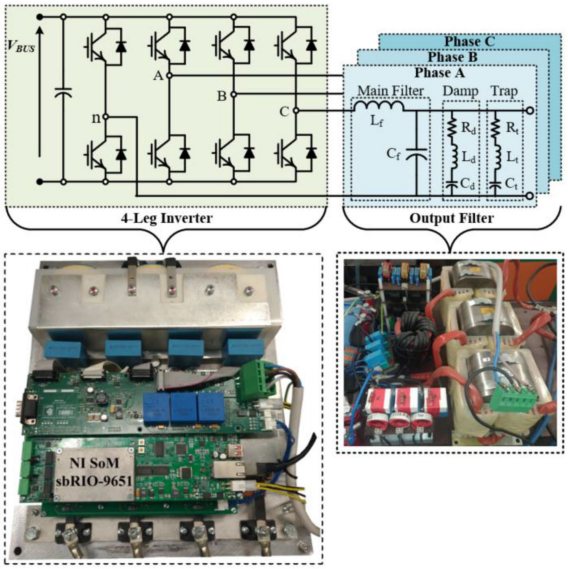

FIGURE 10. Prototype of the 4.leg inverter plus output filter.

A. POWER ELECTRONICS

1) OFF GRID APPLICATIONS (OUTPUT VOLTAGE CONTROL)

Off-grid applications require to comply to strict recommendation on the total harmonic distortion of the voltage (THD_v) provided by the power conversion system. In fact, power quality international standards, such as IEEE STD 519-2014, EN 50160 and IEC 61000-2-4 must be fulfilled by the power converter under different load conditions. Consequently, the power converter must be supported by a proper control structure to obtain high voltage quality. Standalone applications can be referred to the common term of 'AC voltage control'. However, they are not limited to 50 Hz or 60 Hz systems. Ground power units (GPU) for aircrafts is an example of a stand-alone generating unit operating at 400 Hz outputs. To fulfill the mentioned task, the RC structure and its variants have been applied to 40kVA three-phase 4-leg inverter with the output filter [49], [47], [61], as illustrated in Fig. 10.

The converter is composed by four Semikron modules (part number: SEMIX303GB12Vs, 1200V-300A) and the output

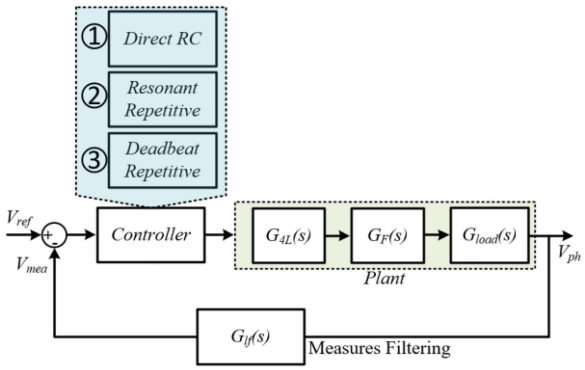

FIGURE 11. Block diagram of the control structure.

filter has three branches: 1) main inductor and capacitors L_f, C_f, damper (R_d, L_d, C_d) branch and trap (R_f, L_f, C_f) branch [62]. Different control strategies have been applied to improve the quality of the converter output voltages: 1) Direct Repetitive control, 2) resonant-repetitive combined control and 3) deadbeat and repetitive control. The block diagram of the control structure is shown in Fig. 11, where $G_{4L}(s)$ is the transfer function (TF) of the 4-leg converter defined in (10), $G_F(s)$ is the TF of the output filter defined in (11), $G_{load}(s)$ is the TF of the equivalent load, $G_{lf}(s)$ is the TF of the second-order low-pass Butterworth filter defined in (12).

$$G_{4L}(s) = k\frac{V_{BUS}}{1 + {}^{s}/_{2\pi f_{sw}}}. \tag{10}$$

$$G_F(s) = \frac{1}{C_f L_f}\frac{s^4 + a_3 s^3 + a_2 s^2 + a_1 s + a_0}{s^6 + b_5 s^5 + b_4 s^4 + b_3 s^3 + b_2 s^2 + b_1 s + b_0}. \tag{11}$$

With filter coefficient

$$a_0 = \frac{1}{C_d C_t L_d L_t}, a_1 = \frac{1}{L_d L_t}\left(\frac{R_d}{C_t} + \frac{R_t}{C_d}\right),$$
$$a_2 = \frac{R_d R_t}{L_d L_t} + \frac{1}{C_t L_t} + \frac{1}{C_d L_d}, a_3 = \frac{R_t}{L_t} + \frac{R_d}{L_d},$$
$$b_0 = \frac{1}{C_d C_f C_t L_d L_f L_t}, b_1 = \frac{1}{C_f L_d L_f L_t}\left(\frac{R_d}{C_t} + \frac{R_t}{C_d}\right),$$
$$b_2 = \frac{1}{C_f C_t L_f L_t} + \frac{1}{C_f C_t L_d L_t} + \frac{1}{C_d C_t L_d L_t} + \frac{1}{C_d C_f L_d L_t} + \frac{1}{C_d C_f L_d L_f} + \frac{R_d R_t}{C_f L_d L_f L_t},$$

$$G_{RR}(z) = \overbrace{\left(1 + K_{rc}\frac{G_f(z)\cdot z^{-N}}{1 - Q(z)\cdot z^{-N}}\right)}^{RCTF}\overbrace{\left(\frac{\left(2k_{ir}\omega_{cr}^2 + 2k_{ir}K_T\omega_{cr}\right)z^2 + \left(4k_{ir}\omega_{cr}^2\right)z + \left(2k_{ir}\omega_{cr}^2 - 2k_{ir}K_T\omega_{cr}\right)}{\left(K_T^2 + 2K_T\omega_{cr} + \omega_0^2 + \omega_{cr}^2\right)z^2 + \left(2\omega_0^2 - K_T^2 + 2\omega_{cr}^2\right)z + \left(K_T^2 - 2K_T\omega_{cr} + \omega_{cr}^2 + \omega_0^2\right)}\right)}^{RSCTF}. \tag{9}$$

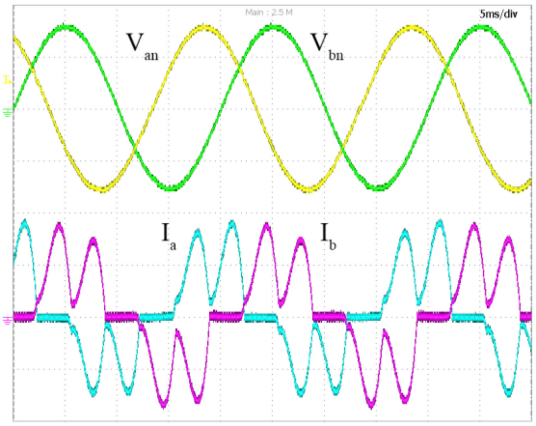

FIGURE 12. Near-zero output voltages THD for 3-phase diode rectifier load. 50 Hz outputs and 12 kHz switching frequency.

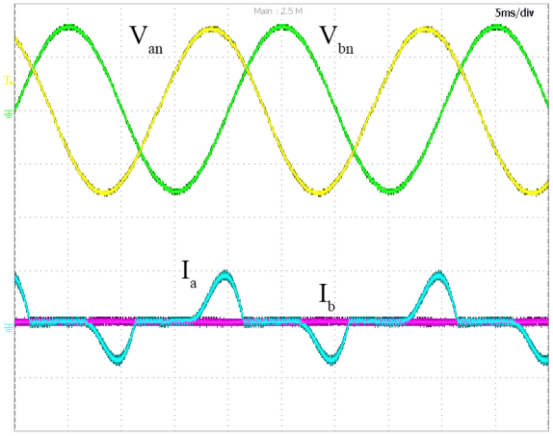

FIGURE 13. Near-zero output voltages THD for 1-phase diode rectifier load. 50 Hz outputs and 12 kHz switching frequency. Phase B and C at no-load.

$$b_3 = \frac{R_d}{C_t L_d L_t} + \frac{R_d}{C_f L_d L_t} + \frac{R_t}{C_f L_f L_t} + \frac{R_d}{C_t L_d L_t} + \frac{R_t}{C_f L_d L_t} + \frac{R_t}{C_d L_d L_t},$$

$$b_4 = \frac{1}{C_t L_t} + \frac{1}{C_f L_f} + \frac{1}{C_f L_d} + \frac{1}{C_d L_f} + \frac{R_d R_t}{L_d},$$

$$b_5 = \frac{R_t}{L_t} + \frac{R_d}{L_d}.$$

$$G_{lf}(s) = \frac{\omega_f^2}{s^2 + \sqrt{2}\omega_f s + \omega_f^2}. \tag{12}$$

Fig. 12 illustrates the voltage and current waveforms in the worst-case condition when a distorting load like a diode rectifier is fed by the system. Fig. 13 show the voltage and current waveforms when a single-phase diode rectifier is connected to the phase A and the other phases are not loaded. In both cases, the direct RC has been selected to track the reference voltages at 50 Hz of the fundamental frequency.

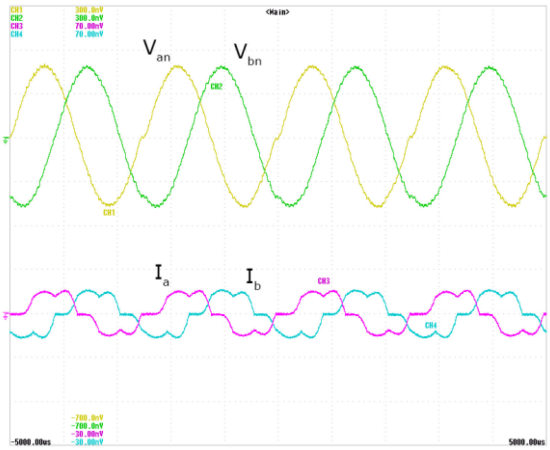

FIGURE 14. GPU application: 400 Hz output and 12 kHz switching frequency. 3-phase diode rectifier load.

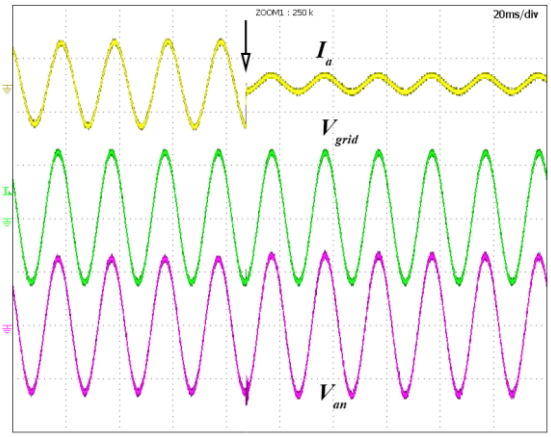

FIGURE 15. Voltage and current waveforms during the transition between off-grid and grid-connected: 3-phase resistive load $R_{load} = 12\ \Omega$, I_a yellow track (20A/div), V_{grid} green track (300V/div), V_{an} magenta track (300V/div).

Fig. 14 shows the waveforms when the direct RC is used to track the reference signal at 400 Hz in the most demanding GPU application. The RC plus the proportional–integral controller is used in [63] to regulate both the output voltage and the output current in case of short-circuit condition. In this case, the control structure adjusts the output voltage in order to obtain a sinusoidal waveform of the output 3Φ5L E-Type Inverter [64] in all load conditions, such as unbalanced and non-linear loads. Fig. 15 shows the voltage and current waveforms during the transition between the off-grid and grid-connected. Particularly, when the converter supplies the three-phase load, the reference voltage is set at 220Vrms. When the converter is connected to the grid, the control algorithm starts to the track the phase current. It is possible to noticed form Fig. 15 that when the converter is connected to the grid, the RC start to adjust the reference current equal to 5 A.

FIGURE 16. Three-phase PFC prototype based on a Hybrid Module.

2) GRID-TIED APPLICATIONS

The repetitive control is also used in grid-tied applications thanks to its brilliant performance to track the reference signals [65]. In [65], the RC is employed with a finite impulse response (FIR) filter, which varies as the grid frequency changes. In this case, the delay time of the RC can be adjusted, and it is linear with frequency due to the FIR. A parallel structure general repetitive control is proposed in [66] to control a grid connected PWM converter. Here, the error convergence rate has been investigated by using the exponential function properties. Furthermore, the proposed parallel structure of RC has been compared to the conventional RC and the dead-beat controllers. The experimental results show an excellent tracking of the phase current with a considerable increase of the current error convergence rate, which results in a faster current controller. In [67] a design guideline of RC used to control the grid connected inverter has been proposed. Here, an admittance model of the inverter-side has been created to facilitate the passivity-based stability assessment and controller parameter optimization. Furthermore, thanks to the plug.in RC, both the reference current tracking accuracy and the quality of the grid injected current has been improved even in the presence of distorted grid conditions.

The digital design of a plug-in RC applied to a three-phase boost rectifier PFC has been proposed at first in [68] applied to the current controllers in a rotating reference frame *dq*; then a combined deadbeat and RC controller in natural coordinates has been developed in [68] showing detailed stability and robustness analysis. Subsequently, in [24] a parallel configuration has been proposed. All the above configurations have considered only constant frequency operation of the AC grid, neglecting its frequency fluctuations. The use of RC in this application permits to mitigate the current harmonics injected into the grid so to comply with THD limits imposed by Grid Standards (e.g., IEC 61000-3-12) even in case of significant grid voltage distortions without increasing the filter inductance values. A plug-in RC, with grid frequency adaptation implemented with the variable delay length approach, has been applied to the three-phase boost rectifier, shown in Fig. 16, based on a Semikron SKiiP25AC12F4V19 1200 V–50 A Hybrid Si-SiC power module. The line inductance filter and output DC capacitance has been sized respectively

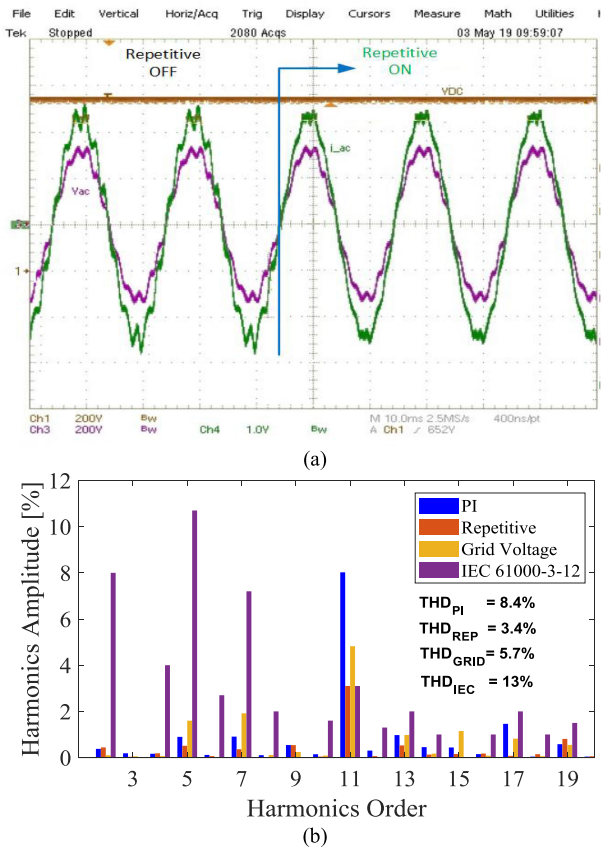

FIGURE 17. Effects of repetitive controller on a phase current under strong grid voltage distortion: (a) AC and DC waveforms: Phase current (green, 10 A/V), Phase Voltage (purple), DC Voltage (brown), (b) harmonics comparison.

to 750 μH and 120 μF. Fractional delay issue due to grid frequency fluctuation can be neglected in this case as the switching frequency is sufficiently high and $f_s = 30$ kHz grid frequency variation is limited (49.5–50.5 Hz), the RC resolution is not significantly affected (T_d/T_s *in range 594–606).* Fig. 17(a) shows the comparison among the line current waveforms achieved with or without RC with strongly distorted grid voltages (THD = 5.7%). Fig. 17(b) highlights the harmonics of the phase currents, obtained with or without RC, in comparison with the maximum values permitted by the standard IEC 61000-3-12; the THD has been reduced from 8.4% to 3.4%.

3) RESONANT PULSED POWER SUPPLY

A resonant pulsed power supply as in Fig. 18 has been proposed in [31] for radio frequency applications to produce as output voltage a series of "long pulses", each one lasting 1ms in time.

For a high-performance power supply, a PI+RC controller is used to impose the following requirements to the output voltages (i.e., V_{out}): 1) the pulse rise time should be less than 100 μs; 2) the pulse overshoot should be less than 3%; 3) the pulse amplitude should be maintained flat along the pulse

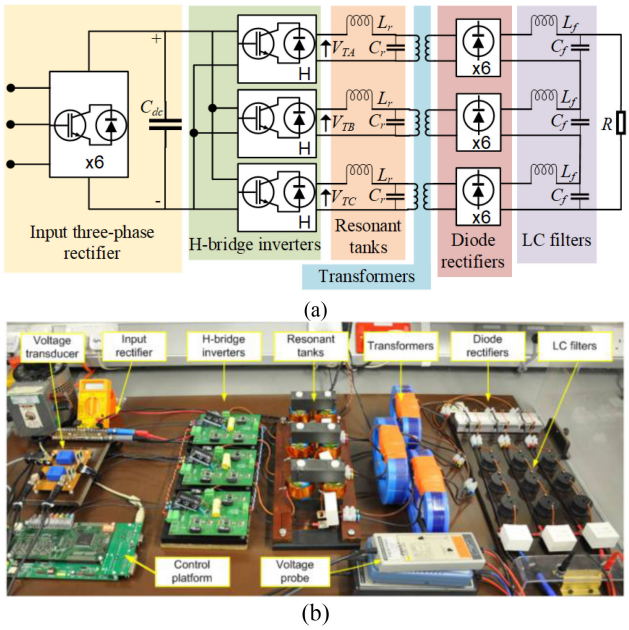

FIGURE 18. **The proposed three-single phase SRPL resonant converter: (a) Block diagram, (b) Experimental rig.**

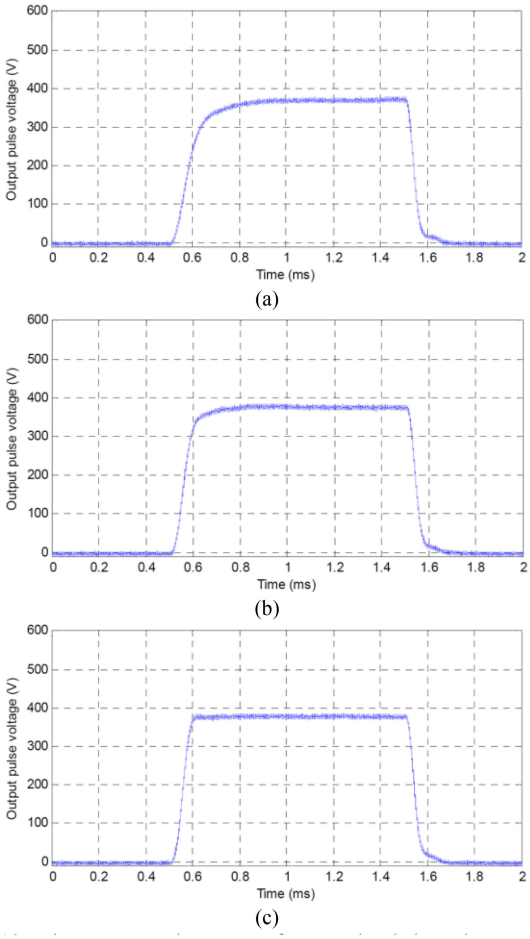

FIGURE 19. **The output voltage waveform under balanced resonant tank condition: (a) with only PI controller, (b) the 2nd period after RC is activated and (c) the 10th period after RC is activated.**

duration, despite the DC-link voltage drops considerably. The equivalent circuit and mathematic model for the control plant can be found in [31], [68]. The feedback PI controller is designed to provide 2 kHz closed loop natural frequency. The RC and PI are connected in the "plug-in" fashion. In order to achieve soft switching, the frequency and phase control proposed in [68] is used in the modulation stage, snubber capacitor is placed across the devices to ensure that the IGBTs in the H-bridge achieve zero crossing point switching on and zero voltage switching off. The experimental test results in Fig. 19 show that the RC can improve the output voltage cycle by cycle under balanced resonant tank condition. The results for unbalanced condition are given in [31].

4) PHASE-LOCKED LOOP

A three-phase phase-locked loop (PLL) is widely used to track in real-time the frequency and phase angle of any three-phase electrical system. The tracked frequency and phase, however, may not be accurate due to harmonic distortions in the three-phase system, unbalances, d.c offsets, grid frequency variations and phase jumps. Although it is desired to design a PLL that can tackle all the aforementioned problems, in order to do so, many existing PLLs often fails to maintain both fast response and low computational burden. According to the analysis in [42], an n^{th} harmonics produces $(n\pm1)^{th}$ harmonic in q-axis voltage, U_q, unbalances produce a 2nd harmonic in U_q, and d.c offsets in U_{abc} produce a 1st harmonic in U_q. Despite these a.c components, accurate frequency and phase tracking can still be achieved if the PLL can force the d.c part of U_q to zero. RC and RO based PLLs have been developed in [42], [69] for both distribution grids and more electrical aircraft (MEA) grids respectively, to cancel the a.c part of U_q. As a result, these two PLLs have achieved superior steady-state performance without sacrificing the fast response while maintaining low computational burden.

For Distribution Grids: The repetitive controller assisted phase-locked loop (RCAPLL) proposed in [42] can be understood as a traditional synchronous rotational frame PLL (SRF-PLL) [70] combined with a variable delay length fractional delay RC. The control diagram is drawn in Fig. 20. In Fig. 20, the PI denotes a traditional proportional-integral controller. The tracked frequency and phase are $\tilde{f}$ and $\tilde{\theta}$ respectively. RC is designed to learn and eventually cancel the a.c part of U_q. As drawn in Fig. 20, the length $\tilde{N}$ is updated in real-time according to the ratio between the sampling frequency f_s and the tracked frequency $\tilde{f}$. Since $\tilde{N}$ can be a fractional number, a 6th order Lagrange fractional delay filter is adopted to implement the fractional delay $z^{-\tilde{N}}$. A moving average filter (MAF) is used to compute the average value of the tracked frequency $\tilde{f}$. In [42], the performance of RCAPLL is tested with a 50 Hz grid which suffers from harmonic distortions, unbalance, dc offsets and phase jump at the same time. The

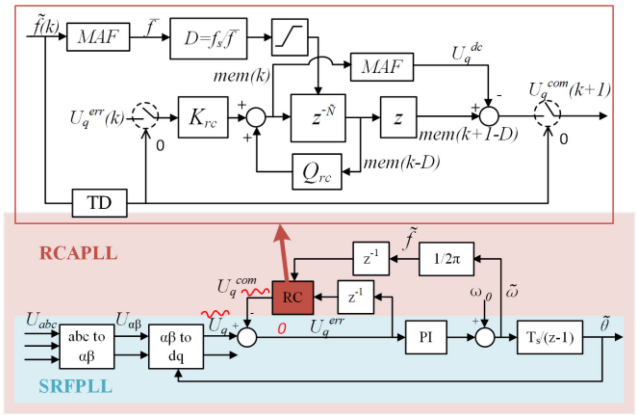

FIGURE 20. Block diagram of the RCAPLL proposed in [38] for three-phase grid.

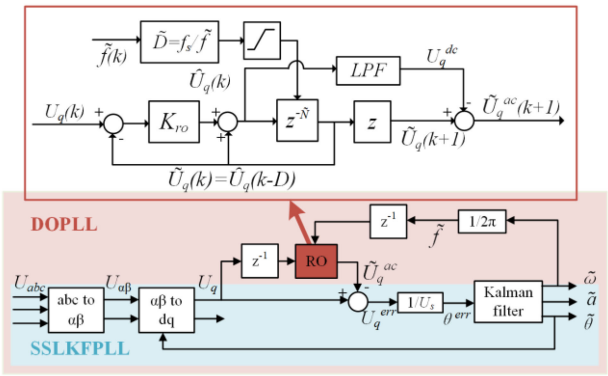

FIGURE 22. Block diagram of the DOPLL proposed in [69] for More Electric Aircraft.

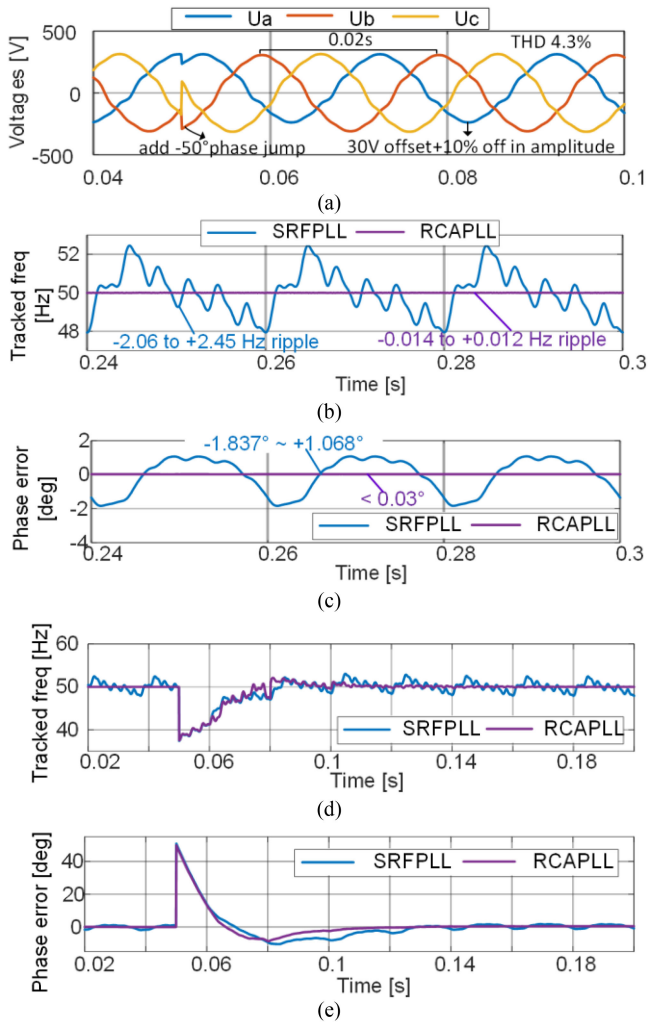

FIGURE 21. Performance of RCAPLL (Additional d.c. offsets of 2.5% in phase A, −0.4% in phase B, 0.2% in phase C and 1.73% unbalance are contained due to sensors and ADC limitations): (a) grid voltage, (b) frequency tracking at steady sate, (c) phase tracking error at steady state, (d) frequency tracking during phase jump, (e) phase tracking error during phase jump.

results in Fig. 21 show that RCAPLL achieves superior frequency and phase tracking at steady state, without scarifying the dynamic performance during phase jumps as its response is as fast as the SRFPLL.

Regarding the grid frequency variation, this method targets standard grid applications where the maximum allowed variation is between 47.5∼51.5 Hz. Applications where grid frequency varies largely, will be discussed in the following section.

For More Electric Aircraft Grids: The grid frequency in More Electric Aircraft (MEA) can vary from 360 to 800 Hz. A dual-observer PLL (DOPLL) has been proposed in [69] combining the third-order model Steady-State Linear Kalman Filter PLL (SSLKFPLL) [71]–[72] and the repetitive observer, as shown in Fig. 22.

The third-order state-space model of the grid is considered as in (E1), being $\theta(k)$, $\omega(k)$ and $a(k)$ the phase, angular frequency and angular frequency acceleration rate of the grid at t_k, respectively. f is the grid frequency in Hz, $\tilde{\tilde{f}}$ is the observed value. Based on (13), the three states can be observer using the Kalman filter as in (14).

$$\begin{bmatrix} \theta(k) \\ \omega(k) \\ a(k) \end{bmatrix} = \mathbf{A} \cdot \begin{bmatrix} \theta(k-1) \\ \omega(k-1) \\ a(k-1) \end{bmatrix}, \mathbf{A} = \begin{bmatrix} 1 & T_s & T_s^2/2 \\ 0 & 1 & T_s \\ 0 & 0 & 1 \end{bmatrix}. \tag{13}$$

$$\begin{bmatrix} \tilde{\theta}(k+1) \\ \tilde{\omega}(k+1) \\ \tilde{a}(k+1) \end{bmatrix} = \mathbf{A} \cdot \left\{ \begin{bmatrix} \tilde{\theta}(k) \\ \tilde{\omega}(k) \\ \tilde{a}(k) \end{bmatrix} + \begin{bmatrix} g_1 \\ g_2 \\ g_3 \end{bmatrix} (\theta(k) - \tilde{\theta}(k)) \right\} \tag{14}$$

The observed phase, angular frequency and angular frequency acceleration are denoted as $\tilde{\theta}$, $\tilde{\omega}$, $\tilde{a}$. The correction gains g_1, g_2, and g_3 can be tuned following the procedures in [73]. The tests in [69] consider a 115 Vrms three-phase grid, of which the grid frequency varies from 360 to 800 Hz following a 500 Hz/s ramp, and from 800 to 360 Hz following a 250 Hz/s ramp according to the maximum allowed variation rate in MIL-STD-704 standard.

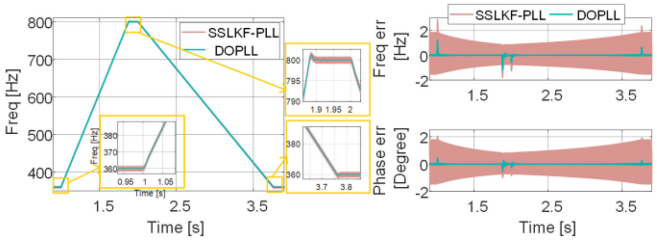

FIGURE 23. Performance of DO-PLL.

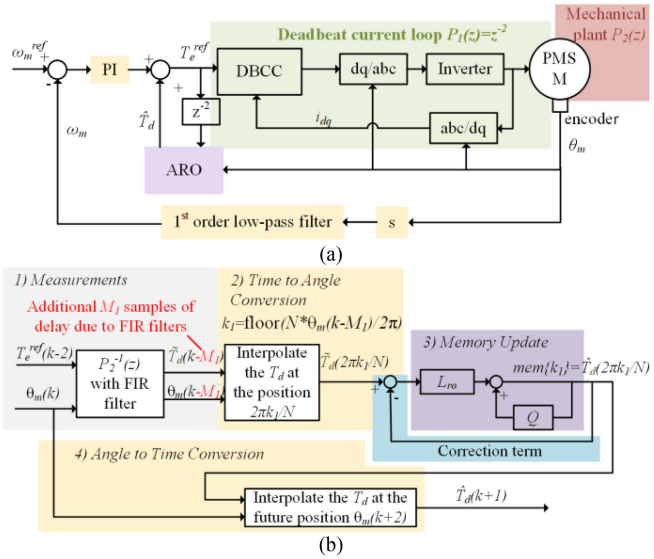

FIGURE 24. Control diagram of ARO for PMSM drives: (a) the overall control diagram and (b) the diagram of ARO.

The same harmonics as in Fig. 21 and +5% offset in phase b, 5% shrinkage in magnitude of phase c have been considered. The simulation results of $\tilde{f}$, $f-\tilde{f}$, θ-$\tilde{\theta}$ are shown in Fig. 23. As demonstrated, significant suppression of harmonics has been achieved using DO-PLL.

B. ELECTRICAL DRIVES

1) TORQUE RIPPLE REDUCTION

In PMSM drives, periodic torque ripple is commonly present due to multiple sources: converter harmonics, cogging effect of the motor, non-sinusoidal flux distribution of the motor, mechanical imperfections, offsets and scaling errors in current feedback. The ripple generated by all these sources is periodic with respect to the rotor position. Since a PMSM drive is likely variable speed, for variable frequency operation, both the angle-based RC (ARC) and the angle-based RO (ARO) have been applied successfully [19], [53]. Among the two methods, the latter method is the most convenient one because there is no need to disable the ARO during speed and load step transients while this is needed when using the ARC.

Fig. 24 shows the control diagram of ARO for PMSM drives as proposed in [53], [54]. Since a deadbeat current controller (DBCC) is used for the current loop, the inner loop can

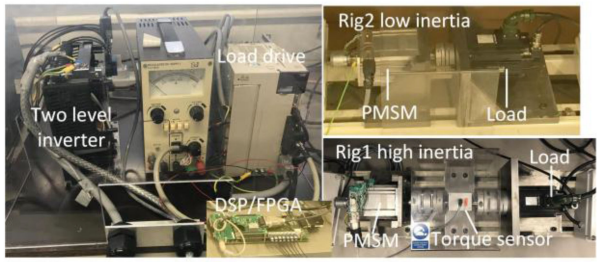

FIGURE 25. Experimental rig for ARO in PMSM drive.

be simplified as $P_1(z)=z^{-2}$. Due to this assumption, $T_e^{ref}(k-2)=T_e(k)$, meaning that the real torque can be estimated by the value of the reference toque with two samples delay. Even if the current loop is non-ideal as previously assumed, this simplification will still be valid since imperfections in the current loop will eventually generate a torque disturbance that will be cancelled by the RO. The angle domain implementation of the RO consists of four steps:

1) Measurements: In the measurements phase, RO estimates the disturbance torque $\tilde{T}_{\rm d}$, where a FIR filter is used to reduce the quantization error of the encoder.
2) Time to angle conversion: In the angle domain, the rotor position $\in[0, 2\pi]$ is divided into N segments. RO only memorizes the error signal when the rotor position is at one of the N chosen locations, i.e., $2\pi i/N$, $i\in[0, N-1]$. Hence, in the time to angle conversion phase, a linear interpolation is used to estimate the disturbance torque at the closest chosen location, $\tilde{T}_{\rm d}(2\pi k_1/N)$, where the equation for k_1 can be seen from Fig. 24.
3) Memory update: An array *mem* of size N is defined to memorize the observed disturbance torque T_d as calculated from (15).

$$\hat{T}_d\left(\frac{2\pi k_1}{N}\right) = mem\{k_1\} = (Q - L_{ro})\cdot mem\{k_1\} + L_{ro}\cdot\tilde{T}_d\left(\frac{2\pi k_1}{N}\right). \quad (15)$$

4) Angle to time conversion: The output of the RO is the estimated torque disturbance at t_{k+2} to compensate two samples of delay in the current loop. Hence, the future position $\theta_m(k+2)$ is estimated by $(\theta_m(k)+2\omega_m T_s)$ and $T_d(\theta_m(k+2))$ is interpolated from *mem* in the angle to time conversion.

The experimental rig and some of the key results in [53] are shown in Figs. 25 and 26.

Fig. 26 confirms that the ARO is effective to reduce torque ripple produced by multiple sources including the 1st and 2nd harmonics (with respect to the electrical frequency) in i_q produced by the current offset and scaling error respectively, 2nd, 4th, 6th harmonics (with respect to the electrical frequency) produced by the odd harmonics in the inverter, the 1st harmonic (with respect to mechanical frequency) produced by mechanical misalignment, and the 12th, 24th, 36th harmonics

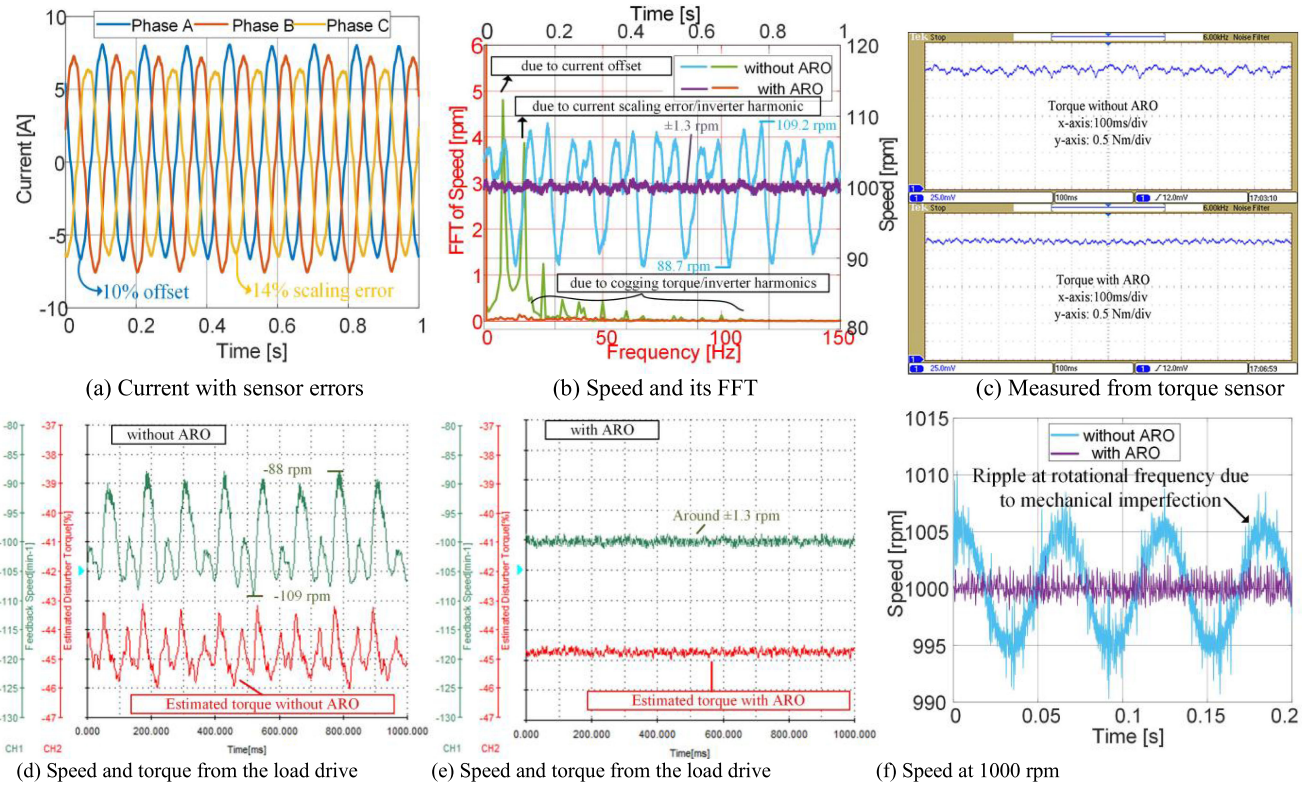

(a) Current with sensor errors (b) Speed and its FFT (c) Measured from torque sensor

(d) Speed and torque from the load drive (e) Speed and torque from the load drive (f) Speed at 1000 rpm

FIGURE 26. Full load test with/without ARO: (a)-(e) at 100 rpms using Rig1 with current sensor errors, (f) at 1000 rpm using Rig2 with mechanical misalignment.

due to the cogging effect created by the 12 slots and teeth. More results on load and speed transients and parameter sensitivity analysis on the mechanical parameters can be found in [53]. Both ARC and ARO are designed to generate the torque reference for canceling the disturbance torque while the DBCC is responsible for tracking such a reference. Alternatively, if the reference torque is generated by other methods, e.g., offline lookup tables, the RC can be used to help tracking the high frequency components in the torque reference. As in [37], the RC is connected in parallel with a PI controller in the current loop.

2) PRECISE POSITION TRACKING

When RC was originally proposed in 1981, it was used for improving the tracking of periodic position reference in servo drives [74]. However, in the state-of-art literature of this field, iterative learning control (ILC) is more frequently mentioned than RC. Although, ILC and RC are proposed by different scientists, and in different years (i.e., ILC is proposed by Uchiyama in 1978 [75]), they are both internal-mode-principle-based theories and have a very similar mathematical definition. The general formulation of ILC is described as (16) in [76].

$$u(t,k) = Q_{ILC}(u(t,k-1)) + L_{ILC}(e(t,k-1)).$$
$$t = 0, 1, \ldots, T-1; k = 1, 2, \ldots. \tag{16}$$

where, $u(t,k)$ denotes the output of the ILC controller at time t, during the k^{th} repeated routine for movement. T is the length of each routine. $e(t, k\text{-}1)$ denotes the control error at t, during the previous (i.e., the $(k\text{-}1)^{\text{th}}$) routine. The function $Q_{ILC}(\cdot)$ is called the Q-filter of ILC, while the function $L_{ILC}(\cdot)$ is called the L-filter of ILC.

Comparing (16) and (1), it can be seen that the Q-filter of ILC is similar to the robustness filter $Q(z)$ of RC, whereas the L-filter of ILC is similar to the gain times the stability filter $k_{rc}G_f(z)$ of RC. For example, the ILC used in [77] for wafer stage positioning can be understood as a plug-in RC. However, in most cases, ILC is designed in a state-space representation according to the survey in [78], while RC is generally designed through a transfer-function approach as compared in [77]. Although both can be applied for repetitive motion control [79]–[84], ILC focuses on batch process, where the movement routine is repetitive.

Whereas RC is more general, and it can be applied whenever periodic tracking error presents. For example, Fig. 27 draws the position loop diagram for a permanent magnet step motor proposed in [83]. Where, k_θ, k_v, k_ω are the position loop proportional and derivative gains and speed loop gain, respectively. θ_m is the rotor position. ω_m is the mechanical speed of the motor. $(\cdot)$ denotes the derivative. $(\sim)$ denotes the tracking error. $(\hat{})$ indicates the estimated value. ψ is the magnetic flux of the motor. It can be seen that the part called "Iterative estimation scheme" is the same as the RC, where

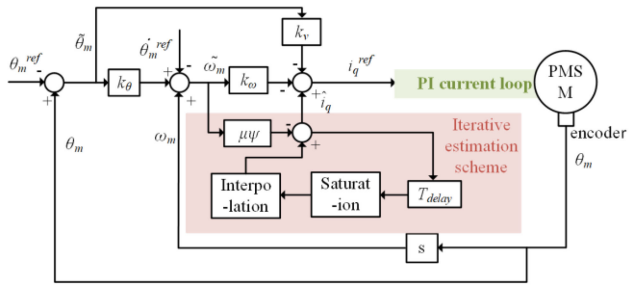

FIGURE 27. Position loop diagram for a permanent magnet step motor with RC resembled estimation scheme as proposed in [83].

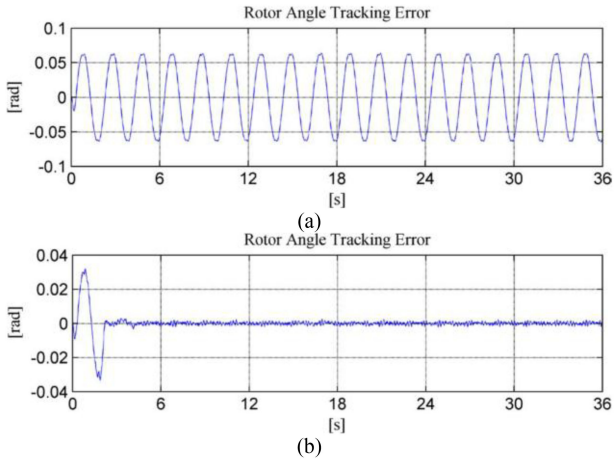

FIGURE 28. Position tracking results of the proposed RC-resembled iterative estimation scheme: (a) with traditional control method, (b) with the RC-resembled iterative estimation scheme.

μ is the gain of RC and T_{delay} is the long delay chain in RC. With the proposed RC-resembled iterative estimation scheme, the rotor angle tracking error of a sine reference can be largely reduced as it is evident in Fig. 28(a) and in Fig. 28(b).

VII. OPEN QUESTIONS AND FUTURE WORK

A. DEALING WITH APERIODIC REFERENCE AND DISTURBANCE

RC is proposed to track periodic reference or to reject periodic disturbance. The main applications are related to all those systems that operate at variable frequency, such as electric drives or waveform generating units. Practically, it is likely that the reference and disturbance may contain not only periodic components, but also aperiodic components. There are potentially two approaches to solve this issue:

1) If the aperiodic reference/disturbance only occurs during certain transients, it would be practical to disable the RC during certain transients in a "detect and switch" manner [19], [85]. Careful considerations should be given to the detection of transients since it varies from application to application.
2) If the aperiodic reference/disturbance occurs randomly, a common solution for aperiodic disturbance is to add an additional equivalent input disturbance (EID) observer [86]–[91] to deal with the aperiodic disturbance, while the RC can focus on the periodic disturbance. Alternatively, it is possible to make the robustness filter $Q(z)$ more adaptive, to remove the aperiodic and random disturbance like in [92].

Overall, it is still an open question whether it is enough to tackle the aperiodic reference/disturbance through using advanced filters inside RC, or it is necessary to add additional control structures to handle this issue for different applications.

B. ADAPTIVE TO NONLINEAR SYSTEM

A system can be nonlinear due to parameter variations or due to discontinuities in the system model. That is the case of many power electronics systems, which changes the operating point and resulting is a modification of their descriptive functions.

The solution can vary according to the impact of the nonlinearity. In the most ideal scenario, the varying parameter could lead to periodic disturbance, which RC is already capable of canceling [93]. Instead, if the impact of the nonlinearity is to produce aperiodic disturbance, the possible solutions are as discussed in the previous subsection. Although, some universal solutions for RC with nonlinear plants are available in literature, most of the papers in this topic are based on ILC. Therefore, further investigation is required to how the methods developed for ILC can be used for RC, such that the methods can be applied for both batched and non-batched (i.e., continuous) process. The available solutions for RC can be categorized into three types according to the type of the plant:

1) NONLINEAR PLANT WITH CONSTANT PARAMETERS

This type of plant can be expressed using a linear differential equation plus a nonlinear bounded disturbance. Adaptive RCs [94] for handling this type of nonlinearity are the most widely studied among the three types.

2) LINEAR PLANT WITH NONLINEAR PARAMETERS

If a *n-th* order plant can be expressed as in (17), where one of the parameters in the system differential equation are non-constant, the system is classified as a linear plant with nonlinear parameters.

$$\begin{cases} x^{(n)} = f(\mathbf{X}, \mathbf{P}_f) + g(\mathbf{X}, p(t))u(t) \\ y = x \end{cases}. \tag{17}$$

where, $\mathbf{X} = [x, x^{(1)}, x^{(2)}, \ldots, x^{(n)}]^{\mathrm{T}} \in \mathbf{R}^n$ is the state vector, $\mathbf{P}_f \in \mathbf{R}^{nf}$ is the unknown constant parameter, $p(t)$ is the unknown time-varying parameter. $f(\cdot)$ and $g(\cdot)$ are the nonlinear functions, $u \in \mathbf{R}$ is the input state, $y \in \mathbf{R}$ is the output state. According to [95], RC can still be applied through proper linearization, but the non/linear parameter variation needs to be sufficiently slow. For multi-input-multi-output system, [96]

has proposed a combination of the high-gain feedback technique and the Nussbaum gain matrix selector to handle the nonlinearity.

3) NONLINEAR PLANT WITH NONLINEAR PARAMETERS

The system state-space equation for such a plant can be expressed as a *n-th* order system in (18).

$$\begin{cases} x^{(n)} = \frac{f(\mathbf{X},\mathbf{P}_f)+g(\mathbf{X},p(t))+u(t)}{b(\mathbf{X},\mathbf{P}_b)} \\ y = x \end{cases} \tag{18}$$

where, $\mathbf{P}_b \in \mathbf{R}^{nb}$ is the unknown constant parameter, $b(\cdot)$ is the nonlinear function.

In order to deal with the case of a nonlinear system with nonlinear parameters, adaptive RCs have been proposed in [97], [98]. Authors in [98] applies a collection of fuzzy if-then rules to approximate the input of RC. In such way, the approximated input of RC is model-free, and the nonlinear parameterization will not affect the RC. Meanwhile, the parameters in RC are updated by an adaptive law derived from the Lyapunov synthesis method to ensure stability.

C. SMART TUNING METHOD BASED ON RC

The Smart Tuning approach based on RC takes the benefits and the characteristics of Iterative-Learning algorithms to provide a help in the controllers parameters tuning for different control structures. This methodology could find application in many conversion systems due to the sure presence of a control algorithm.

In [99], a combination of RC and proportional-integral-derivative (PID) control actions has been studied, where the output of RC is added to the reference signal and the PID controller is used as the feedback controller. Interestingly, it is derived in [99] that such a structure is equivalent to two PID controllers connected in parallel, where one PID controller is the same as the original PID controller, while the second is an adaptive PID controller with gains iteratively updated by the RC. Hence, the second PID is effectively tuned by the RC control law. This opens a new direction of research to investigate the use of the RC control law to tune other controllers, so that they can inherit the learning ability of RC.

VIII. CONCLUSION

This paper has provided a broad review on the state of the art of RC used in power electronics and drives. At first the underlying concepts on RC have been highlighted and explained, together with its different structures; in addition, the RC control design methods and its implementation on DSP and LabVIEW FPGA have been discussed. Structure and design of RC have also been provided for both fixed and variable frequency operating conditions. In the second part of the paper, more recent and optimized control approaches based on RC have been examined for power electronics and drive systems. In particular, the combination of RC with resonant control, the combination of RC with deadbeat control, as well as the RC in conjunction with disturbance observer have been provided. Additionally, several examples of RC used in power electronics and electric drives developed in recent years have been discussed. RC definitely represents a very effective approach in directly controlling variables which present a periodic behavior (or rejecting periodic disturbance) and can also be successfully used as support to other control systems to improve steady state regulation performance. Power Electronics and Electrical drives for their intrinsic characteristics represent a natural application for RC-based control systems, as the many successful examples illustrated in this paper clearly demonstrate.

REFERENCES

[1] A. Garcia-Cerrada, O. Pinzon-Ardila, V. Feliu-Batlle, P. Roncero-Sanchez, and P. Garcia-Gonzalez, "Application of a repetitive controller for a three-phase active power filter," *IEEE Trans. Power Electron.*, vol. 22, no. 1, pp. 237–246, Jan. 2007.

[2] S. Hara, Y. Yamamoto, T. Omata, and M. Nakano, "Repetitive control system: A new type servo system for periodic exogenous signals," *IEEE Trans. Autom. Control*, vol. 33, no. 7, pp. 659–668, Jul. 1988.

[3] W. Meng, S. Q. Xie, Q. Liu, C. Z. Lu, and Q. Ai, "Robust iterative feedback tuning control of a compliant rehabilitation robot for repetitive ankle training," *IEEE/ASME Trans. Mechatronics*, vol. 22, no. 1, pp. 173–184, Feb. 2017.

[4] A. Tayebi, S. Abdul, M. B. Zaremba, and Y. Ye, "Robust iterative learning control design: Application to a robot manipulator," *IEEE/ASME Trans. Mechatronics*, vol. 13, no. 5, pp. 608–613, Oct. 2008.

[5] H. Liao, M. J. Roelle, J. Chen, S. Park, and J. C. Gerdes, "Implementation and analysis of a repetitive controller for an electro-hydraulic engine valve system," *IEEE Trans. Control Syst. Technol.*, vol. 19, no. 5, pp. 1102–1113, Sep. 2011.

[6] J. D. Álvarez, L. J. Yebra, and M. Berenguel, "Repetitive control of tubular heat exchangers," *J. Process Control*, vol. 17, no. 9, pp. 689–701, Feb. 2007.

[7] G. Pandove and M. Singh, "Robust repetitive control design for a three-phase four wire shunt active power filter," *IEEE Trans. Ind. Inform.*, vol. 15, no. 5, pp. 2810–2818, May 2019.

[8] Y. Yang, K. Zhou, and F. Blaabjerg, "Enhancing the frequency adaptability of periodic current controllers with a fixed sampling rate for grid-connected power converters," *IEEE Trans. Power Electron.*, vol. 31, no. 10, pp. 7273–7285, Oct. 2016.

[9] S. Yang, P. Wang, Y. Tang, M. Zagrodnik, X. Hu, and K. J. Tseng, "Circulating current suppression in modular multilevel converters with even-harmonic repetitive control," *IEEE Trans. Ind. Appl.*, vol. 54, no. 1, pp. 298–309, Jan./Feb. 2018.

[10] G. A. Ramos and R. Costa-Castelló, "Power factor correction and harmonic compensation using second-order odd-harmonic repetitive control," *IET Control Theory Appl.*, vol. 6, no. 11, pp. 1633–1644, Jul. 2012.

[11] S. Xiong and D. B. Bogy, "Hard disk drive servo system based on field-programmable gate arrays," *IEEE Trans. Ind. Electron.*, vol. 61, no. 9, pp. 4878–4884, Sep. 2014.

[12] G. Pipeleers, B. Demeulenaere, J. D. Schutter, and J. Swevers, "Generalised repetitive control: Relaxing the period-delay-based structure," *IET Control Theory Appl.*, vol. 3, no. 11, pp. 1528–1536, Nov. 2009.

[13] K. Chang, I. Shim, and G. Park, "Adaptive repetitive control for an eccentricity compensation of optical disk drivers," *IEEE Trans. Consum. Electron.*, vol. 52, no. 2, pp. 445–450, May 2006.

[14] G. Escobar, G. A. Catzin-Contreras, and M. J. Lopez-Sanchez, "Compensation of variable fractional delays in the 6k±1 repetitive controller," *IEEE Trans. Ind. Electron.*, vol. 62, no. 10, pp. 6448–6456, Oct. 2015.

[15] Z. Cao and G. F. Ledwich, "Adaptive repetitive control to track variable periodic signals with fixed sampling rate," *IEEE/ASME Trans. Mechatronics*, vol. 7, no. 3, pp. 378–384, Sep. 2002.

[16] Z. Zou, K. Zhou, Z. Wang, and M. Cheng, "Frequency-Adaptive fractional-order repetitive control of shunt active power filters," *IEEE Trans. Ind. Electron.*, vol. 62, no. 3, pp. 1659–1668, Mar. 2015.

[17] M. A. Herran, J. R. Fischer, S. A. González, M. G. Judewicz, I. Carugati, and D. O. Carrica, "Repetitive control with adaptive sampling frequency for wind power generation systems," *IEEE J. Emerg. Sel. Topics Power Electron.*, vol. 2, no. 1, pp. 58–69, Mar. 2014.

[18] P. Zanchetta, M. Degano, J. Liu, and P. Mattavelli, "Iterative learning control with variable sampling frequency for current control of grid-connected converters in aircraft power systems," *IEEE Trans. Ind. Appl.*, vol. 49, no. 4, pp. 1548–1555, Jul./Aug. 2013.

[19] M. Tang, A. Gaeta, A. Formentini, and P. Zanchetta, "A fractional delay variable frequency repetitive control for torque ripple reduction in PMSMs," *IEEE Trans. Ind. Appl.*, vol. 53, no. 6, pp. 5553–5562, Nov./Dec. 2017.

[20] M. Tomizuka, "Zero phase error tracking algorithm for digital control," *J. Dynamic Syst. Meas. Control*, vol. 109, pp. 65–68, 1987.

[21] B. Zhang, D. Wang, K. Zhou, and Y. Wang, "Linear phase lead compensation repetitive control of a CVCF PWM inverter," *IEEE Trans. Ind. Electron.*, vol. 55, no. 4, pp. 1595–1602, Apr. 2008.

[22] A. Lidozzi, L. Solero, F. Crescimbini, C. Ji, S. Bifaretti, and P. Zanchetta, "FPGA-based direct repetitive control for high performance ground power units," in *Proc. IEEE Energy Convers. Congr. Expo.*, Cincinnati, OH, USA, 2017, pp. 3063–3068.

[23] M.-C. Tsai and W.-S. Yao, "Design of a plug-in type repetitive controller for periodic inputs," *IEEE Trans. Control Syst. Technol.*, vol. 10, no. 4, pp. 547–555, Jul. 2002.

[24] X. H. Wu, S. K. Panda, and J. X. Xu, "Design of a plug-in repetitive control scheme for eliminating supply-side current harmonics of three-phase PWM boost rectifiers under generalized supply voltage conditions," *IEEE Trans. Power Electron.*, vol. 25, no. 7, pp. 1800–1810, Jul. 2010.

[25] C. Weijie, X. Fangchun, W. Min, and S. Jinhua, "Design of a repetitive control system based on the compensation of nonlinearities," in *Proc. 32nd Chin. Control Conf.*, Xi'an, China, 2013, pp. 182–186.

[26] E. Kurniawan, Z. Cao, and Z. Man, "Digital design of adaptive repetitive control of linear systems with time-varying periodic disturbances," *IET Control Theory Appl.*, vol. 8, no. 17, pp. 1995–2003, 2014.

[27] W. E. Dixon, E. Zergeroglu, D. M. Dawson, and B. T. Costic, "Repetitive learning control: A Lyapunov-based approach," *IEEE Trans. Syst. Man. Cybern. Part B (Cybernetics)*, vol. 32, no. 4, pp. 538–545, Aug. 2002.

[28] J.-X. Xu and J. Xu, "Observer based learning control for a class of nonlinear systems with time-varying parametric uncertainties," *IEEE Trans. Autom. Control*, vol. 49, no. 2, pp. 275–281, Feb. 2004.

[29] M. Wu, L. Zhou, and J. She, "Design of observer-based H_∞ robust repetitive-control system," *IEEE Trans. Autom. Control*, vol. 56, no. 6, pp. 1452–1457, Jun. 2011.

[30] A. Noshadi, J. Shi, W. S. Lee, P. Shi, and A. Kalam, "Repetitive disturbance observer-based control for an active magnetic bearing system," in *2015 5th Australian Control Conf.*, Gold Coast, QLD, Australia, 2015, pp. 55–60.

[31] C. Ji, P. Zanchetta, F. Carastro, and J. Clare, "Repetitive control for high-performance resonant pulsed power supply in radio frequency applications," *IEEE Trans. Ind. Appl.*, vol. 50, no. 4, pp. 2660–2670, Jul./Aug. 2014.

[32] M. Yamada, Z. Riadh, and Y. Funahashi, "Design of discrete-time repetitive control system for pole placement and application," *IEEE/ASME Trans. Mechatronics*, vol. 4, no. 2, pp. 110–118, Jun. 1999.

[33] E. Kurniawan, Z. Cao, and Z. Man, "Design of robust repetitive control with time-varying sampling periods," *IEEE Trans. Ind. Electron.*, vol. 61, no. 6, pp. 2834–2841, Jun. 2014.

[34] E. Kurniawan, Z. Cao, and Z. Man, "Design of decentralized repetitive control of linear MIMO system," in *Proc. IEEE 8th Conf. Ind. Electron. Appl.*, Melbourne, VIC, Australia, 2013, pp. 427–432.

[35] R. Costa-Castelló, J. Nebot, and R. Grinó, "Demonstration of the internal model principle by digital repetitive control of an educational laboratory plant," *IEEE Trans. Educ.*, vol. 48, no. 1, pp. 73–80, Feb. 2005.

[36] M. Tomizuka, T.-C. Tsao, and K.-K. Chew, "Discrete-time domain analysis and synthesis of repetitive controllers," in *Proc. 1988 Amer. Control Conf.*, Atlanta, GA, USA, 1988, pp. 860–866.

[37] P. Mattavelli, L. Tubiana, and M. Zigliotto, "Torque-ripple reduction in PM synchronous motor drives using repetitive current control," *IEEE Trans. power Electron.*, vol. 20, no. 6, pp. 1423–1431, Nov. 2005.

[38] K. K. Chew and M. Tomizuka, "Digital control of repetitive errors in disk drive systems," *Control Syst. Mag. IEEE*, vol. 10, , no. 1, pp. 16–20, Jan. 1990.

[39] K. Zhou, D. Wang, and K.-S. Low, "Periodic errors elimination in CVCF PWM DC/AC converter systems: Repetitive control approach," *IEE Proc.-Control Theory Appl.*, vol. 147, no. 6, pp. 694–700, Nov. 2000.

[40] Z. Liu, B. Zhang, and K. Zhou, "Universal fractional-order design of linear phase lead compensation multirate repetitive control for PWM inverters," *IEEE Trans. Ind. Electron.*, vol. 64, no. 9, pp. 7132–7140, Sep. 2017.

[41] Y. Yang, K. Zhou, H. Wang, F. Blaabjerg, D. Wang, and B. Zhang, "Frequency adaptive selective harmonic control for grid-connected inverters," *IEEE Trans. Power Electron.*, vol. 30, no. 7, pp. 3912–3924, Jul. 2015.

[42] M. Tang, S. Bifaretti, S. Pipolo, S. Odhano, and P. Zanchetta, "A novel repetitive controller assisted phase-locked loop with self-learning disturbance rejection capability for three-phase grids," *IEEE J. Emerg. Sel. Topics Power Electron.*, vol. 8, no. 2, Jun. 2020, pp. 1870–1879.

[43] W. Lu, K. Zhou, D. Wang, and M. Cheng, "A generic digital nk±m order harmonic repetitive control scheme for PWM converters," *IEEE Trans. Ind. Electron.*, vol. 61, no. 3, pp. 1516–1527, Mar. 2014.

[44] Y. Ye, Y. Wu, G. Xu, and B. Zhang, "Cyclic repetitive control of CVCF PWM DC–AC converters," *IEEE Trans. Ind. Electron.*, vol. 64, no. 12, pp. 9399–9409, Dec. 2017.

[45] V. Salis *et al.*, "Padé-based-repetitive learning current-control for voltage source inverters," in *Proc. IEEE Energy Convers. Congr. Expo.*, Portland, OR, USA, 2018, pp. 1473–1477.

[46] S. L. Jung, H. S. Huang, and Y. Y. Tzou, "A three-phase PWM AC–DC converter with low switching frequency and high power factor using DSP-based repetitive control technique," in *Proc. IEEE PESC'98 Conf.*, Fukuoka, Japan, 1998, pp. 517–523.

[47] A. Lidozzi, C. Ji, L. Solero, P. Zanchetta, and F. Crescimbini, "Digital deadbeat and repetitive combined control for a stand-alone four-leg VSI," *IEEE Trans. Ind. Appl.*, vol. 53, no. 6, pp. 5624–5633, Nov./Dec. 2017.

[48] E. Kurniawan, Z. Cao, and Z. Man, "Design of robust repetitive control with time-varying sampling periods," *IEEE Trans. Ind. Electron.*, vol. 61, no. 6, pp. 2834–2841, Jun. 2014.

[49] A. Lidozzi, C. Ji, L. Solero, P. Zanchetta, and F. Crescimbini, "Resonant–repetitive combined control for stand-alone power supply units," *IEEE Trans. Ind. Appl.*, vol. 51, no. 6, pp. 4653–4663, Nov./Dec. 2015.

[50] C. Blanco, F. Tardelli, D. Reigosa, P. Zanchetta, and F. Briz, "Design of a cooperative voltage harmonic compensation strategy for islanded microgrids combining virtual admittance and repetitive controller," *IEEE Trans. Ind. Appl.*, vol. 55, no. 1, pp. 680–688, Jan./Feb. 2019.

[51] A. G. Yepes, F. D. Freijedo, J. Doval-Gandoy, Ó. López, J. Malvar, and P. Fernandez-Comesaña, "Effects of discretization methods on the performance of resonant controllers," *IEEE Trans. Power Electron.*, vol. 25, no. 7, pp. 1692–1712, Jul. 2010.

[52] S. Madichetty, M. Basu, S. Mishra, and J. M. Guerrero, "Double deadbeat plus repetitive control scheme for microgrid system," *IEEE Syst. J.*, vol. 13, no. 3, pp. 3194–3202, Sep. 2019.

[53] M. Tang, A. Formentini, S. A. Odhano, and P. Zanchetta, "Torque ripple reduction of PMSMs using a novel angle-based repetitive observer," *IEEE Trans. Ind. Electron.*, vol. 67, no. 4, pp. 2689–2699, Apr. 2020.

[54] M. Tang, A. Formentini, and P. Zanchetta, "Repetitive observer design for torque ripple reduction in PMSM drives," in *Proc. 21st Eur. Conf. Power Electron. Appl. (EPE'19 ECCE Europe*), Genova, Italy, 2019, pp. 1–9.

[55] M. Tang, A. Formentini, S. Odhano, and P. Zanchetta, "Design of a repetitive controller as a feed-forward disturbance observer," in *Proc. IECON 2016-42nd Annu. Conf. IEEE Ind. Electron. Soc.*, Florence, Italy, 2016, pp. 78–83.

[56] S. Lee, W. Cha, B. Kwon, and M. Kim, "Discrete-time repetitive control of flyback CCM inverter for PV power applications," *IEEE Trans. Ind. Electron.*, vol. 63, no. 2, pp. 976–984, Feb. 2016.

[57] Y. Jeong, S. Lee, S. Jeong, J. Kwon, and B. Kwon, "High-efficiency bidirectional grid-tied converter using single power conversion with high-quality grid current," *IEEE Trans. Ind. Electron.*, vol. 64, no. 11, pp. 8504–8513, Nov. 2017.

[58] B. Han, J. S. Lee, and M. Kim, "Repetitive controller with phase-lead compensation for cuk CCM inverter," *IEEE Trans. Ind. Electron.*, vol. 65, no. 3, pp. 2356–2367, Mar. 2018.

[59] R. Grino, R. Cardoner, R. Costa-Castello, and E. Fossas, "Digital repetitive control of a three-phase four-wire shunt active filter," *IEEE Trans. Ind. Electron.*, vol. 54, no. 3, pp. 1495–1503, Jun. 2007.

[60] G. Pandove and M. Singh, "Robust repetitive control design for a three-phase four wire shunt active power filter," *IEEE Trans. Ind. Inform.*, vol. 15, no. 5, pp. 2810–2818, May 2019.

[61] A. Lidozzi, C. Ji, L. Solero, F. Crescimbini, and P. Zanchetta, "Load-Adaptive zero-phase-shift direct repetitive control for stand-alone four-leg VSI," *IEEE Trans. Ind. Appl.*, vol. 52, no. 6, pp. 4899–4908, Nov./Dec. 2016.

[62] G. Lo Calzo, A. Lidozzi, L. Solero, and F. Crescimbini, "LC filter design for on-grid and off-grid distributed generating units," *IEEE Trans. Ind. Appl.*, vol. 51, no. 2, pp. 1639–1650, Mar./Apr. 2015.

[63] M. Di Benedetto, A. Lidozzi, L. Solero, F. Crescimbini, and P. J. Grbovic, "Concurrent control for three-phase four-wire five levels E-Type inverter for microgrids," in *Proc. IEEE Energy Convers. Congr. Expo.*, Portland, OR, USA, 2018, pp. 202–207.

[64] M. di Benedetto, A. Lidozzi, L. Solero, F. Crescimbini, and P. J. Grbović, "Low volume and low weight 3-phase 5-level back to back E-Type converter," *IEEE Trans. Ind. Appl.*, vol. 55, no. 6, pp. 7377–7388, Nov./Dec. 2019.

[65] D. Chen, J. Zhang, and Z. Qian, "An improved repetitive control scheme for grid-connected inverter with frequency-adaptive capability," *IEEE Trans. Ind. Electron.*, vol. 60, no. 2, pp. 814–823, Feb. 2013.

[66] W. Lu, K. Zhou, M. Cheng, J. Shen, and L. Wu, "Parallel structure general repetitive controller for general grid-connected PWM converters," *IET Power Electron.*, vol. 10, no. 3, pp. 338–347, Mar. 2017.

[67] C. Xie, D. Liu, K. Li, J. Zou, K. Zhou, and J. M. Guerrero, "Passivity-Based design of repetitive controller for LCL-type grid-connected inverters suitable for microgrid applications," *IEEE Trans. Power Electron.*, vol. 36, no. 2, pp. 2420–2431, Feb. 2021.

[68] K. Zhou and D. Wang, "Digital repetitive controlled three-phase PWM rectifier," *IEEE Trans. Power Electron.*, vol. 18, no. 1, pp. 309–316, Jan. 2003.

[69] M. Tang, S. Bifaretti, S. Pipolo, A. Formentini, O. S, and P. Zanchetta, "Disturbance rejection ability enhancement using repetitive observer in phase-locked loop for more electric aircraft," in *Proc. IEEE Energy Convers. Congr. Expo.*, Detroit, MI, USA, 2020, pp. 6379–6384.

[70] F. González-Espín, E. Figueres, and G. Garcerá, "An adaptive synchronous-reference-frame phase-locked loop for power quality improvement in a polluted utility grid," *IEEE Trans. Ind. Electron.*, vol. 59, no. 6, pp. 2718–2731, Jun. 2012.

[71] H. Wang, P. Zanchetta, J. Clare, and C. Ji, "Modelling and control of a zero current switching high-voltage resonant converter power supply for radio frequency sources," *IET Power Electron.*, vol. 5, no. 4, pp. 401–409, 2012.

[72] A. Bellini, S. Bifaretti, and V. Iacovone, "Robust PLL algorithm for three-phase grid-connected converters," *EPE J.*, vol. 20, no. 4, pp. 22–30, 2010.

[73] S. Bifaretti, A. Lidozzi, L. Solero, and F. Crescimbini, "Anti-islanding detector based on a robust PLL," *IEEE Trans. Ind. Appl.*, vol. 51, no. 1, pp. 398–405, Jan./Feb. 2015.

[74] T. Inoue, M. Nakano, and S. Iwai, "High accuracy control of servomechanism for repeated contouring," in *Proc. 10th Annu. Symp. Incremental Motion Control Syst. Devices*, Urbana-Champaign, USA, 1981, pp. 285–292.

[75] M. Uchiyama, "Formulation of high-speed motion pattern of a mechanical arm bytrial," (in Japanese), *Trans. Soc. Instrum. Control Eng.*, vol. 4, pp. 706–712, 1978.

[76] Y. Wang, F. Gao, and F. J. Doyle, "Survey on iterative learning control, repetitive control, and run-to-run control," *J. Process Control*, vol. 19, no. 10, pp. 1589–1600, 2009.

[77] P. Y. H.Hashimoto *et al.*, "Precision and settling time improvement for the wafer stage of lithography scanners with iterative learning control," in *Proc. 1st Int. Conf. Positioning Technol.*, Hamamatsu, Japan, 2004.

[78] D. A. Bristow, M. Tharayil, and A. G. Alleyne, "A survey of iterative learning control," *IEEE control Syst. Mag.*, vol. 26, no. 3, pp. 96–114, Jun. 2006.

[79] K. Kaneko and R. Horowitz, "Repetitive and adaptive control of robot manipulators with velocity estimation," *IEEE Trans. Robot. Automat.*, vol. 13, no. 2, pp. 204–217, Apr. 1997.

[80] J. Yao, Z. Jiao, and D. Ma, "A practical nonlinear adaptive control of hydraulic servomechanisms with periodic-like disturbances," *IEEE/ASME Trans. Mechatronics*, vol. 20, no. 6, pp. 2752–2760, Dec. 2015.

[81] X. Li *et al.*, "Data-driven multi-objective controller optimization for a magnetically-levitated nanopositioning system," *IEEE/ASME Trans. Mechatronics*, vol. 25, no. 4, pp. 1961–1970, Aug. 2020.

[82] L. Biagiotti, F. Califano, and C. Melchiorri, "Repetitive control meets continuous zero phase error tracking controller for precise tracking of B-Spline trajectories," *IEEE Trans. Ind. Electron.*, vol. 67, no. 9, pp. 7808–7818, Sep. 2020.

[83] S. Bifaretti, V. Iacovone, A. Rocchi, P. Tomei, and C. M. Verrelli, "Global learning position controls for permanent-magnet step motors," *IEEE IEEE Trans. Ind. Electron.*, vol. 58, no. 10, pp. 4654–4663, Oct. 2011.

[84] S. Bifaretti, P. Tomei, and C. M. Verrelli, "A global robust iterative learning position control for current-fed permanent magnet step motors," in *Proc. IEEE Int. Symp. Ind. Electron.*, Bari, Italy, 2010, pp. 30–35.

[85] L. Ott, F. Nageotte, P. Zanne, and M. de Mathelin, "Physiological motion rejection in flexible endoscopy using visual servoing and repetitive control: Improvements on non-periodic reference tracking and non-periodic disturbance rejection," in *Proc. IEEE Int. Conf. Robot. Automat.*, Kobe, Japan, 2009, pp. 4233–4238.

[86] L. Zhou, J. She, Y. He, and C. Li, "Aperiodic disturbance rejection in a modified repetitive-control system with non-linear uncertainty," *IET Control Theory Appl.*, vol. 10, no. 18, pp. 2394–2402, Dec. 2016.

[87] R. Sakthivel, K. Raajananthini, F. Alzahrani, and B. Kaviarasan, "Observer-based modified repetitive control for fractional-order nonlinear systems with unknown disturbances," *IET Control Theory Appl.*, vol. 13, no. 18, pp. 3132–3138, Dec. 2019.

[88] M. Wu, B. Xu, W. Cao, and J. She, "Aperiodic disturbance rejection in repetitive-control systems," *IEEE Trans. Control Syst. Technol.*, vol. 22, no. 3, pp. 1044–1051, May 2014.

[89] R. Sakthivel, S. Mohanapriya, H. R. Karimi, and P. Selvaraj, "A robust repetitive-control design for a class of uncertain stochastic dynamical systems," *IEEE Trans. Circuits Syst. II: Exp. Briefs*, vol. 64, no. 4, pp. 427–431, Apr. 2017.

[90] L. Zhou, J. She, Y. H. Minwu, and S. Zhou, "Estimation and rejection of aperiodic disturbance in a modified repetitive-control system," *IET Control Theory Appl.*, vol. 8, no. 10, pp. 882–889, Jul. 2014.

[91] A. H. M. Sayem, Z. Cao, and Z. Man, "Model free ESO-based repetitive control for rejecting periodic and aperiodic disturbances," *IEEE Trans. Ind. Electron.*, vol. 64, no. 4, pp. 3433–3441, Apr. 2017.

[92] K. Kalyanam and T. Tsao, "Two-Period repetitive and adaptive control for repeatable and nonrepeatable runout compensation in disk drive track following," *IEEE/ASME Trans. Mechatronics*, vol. 17, no. 4, pp. 756–766, Aug. 2012.

[93] R. A. Mastromauro, M. Liserre, and A. Dell'Aquila, "Study of the effects of non-linear inductance on the performance of resonant and repetitive controllers," in *Proc. IEEE Int. Symp. Ind. Electron.*, 2006, pp. 1498–1503.

[94] M. Sun, S. S. Ge, and I. M. Y. Mareels, "Adaptive repetitive learning control of robotic manipulators without the requirement for initial repositioning," *IEEE Trans. Robot.*, vol. 22, no. 3, pp. 563–568, Jun. 2006.

[95] J. Ghosh and B. Paden, "Nonlinear repetitive control," *IEEE Trans. Autom. Control*, vol. 45, no. 5, pp. 949–954, May 2000.

[96] Z. Yang, S. C. P. Yam, L. K. Li, and Y. Wang, "Universal repetitive learning control for nonparametric uncertainty and unknown state-dependent control direction matrix," *IEEE Trans. Autom. Control*, vol. 55, no. 7, pp. 1710–1715, Jul. 2010.

[97] M. Sun and S. S. Ge, "Adaptive repetitive control for a class of nonlinearly parametrized systems," *IEEE Trans. Autom. Control*, vol. 51, no. 10, pp. 1684–1688, Oct. 2006.

[98] W. Sun, H. Cai, and F. Zhao, "FBFN-based adaptive repetitive control of nonlinearly parameterized systems," *J. Syst. Eng. Electron.*, vol. 24, no. 6, pp. 1003–1010, Dec. 2013.

[99] K. K. Tan, S. Zhao, and J. Xu, "Online automatic tuning of a proportional integral derivative controller based on an iterative learning control approach," *IET Control Theory Appl.*, vol. 1, no. 1, pp. 90–96, Jan. 2007.